

Dimensionality affects extinction of bistable populations

Yifei Li¹, Stuart T. Johnston², Pascal R. Buenzli¹, Peter van Heijster³, Matthew J. Simpson¹

¹*School of Mathematical Sciences, Queensland University of Technology, Brisbane, Australia.*

²*Systems Biology Laboratory, School of Mathematics and Statistics, and Department of Biomedical Engineering, Melbourne School of Engineering, University of Melbourne, Parkville, Victoria, Australia.*

³*Biometris, Wageningen University and Research, Wageningen, The Netherlands.*

Abstract

The question of whether biological populations survive or are eventually driven to extinction has long been examined using mathematical models. In this work we study population survival or extinction using a stochastic, lattice—based random walk model where individuals undergo migration, birth and death events. The stochastic model is defined on a two—dimensional hexagonal lattice with periodic boundary conditions. A key feature of the stochastic model is that crowding effects are introduced by specifying two different crowding functions that govern how local agent density influences migration events and birth/death events. The continuum limit description of the stochastic model is a nonlinear reaction—diffusion equation, and in this work we focus on crowding functions that lead to linear diffusion and a bistable reaction term that is often associated with the strong Allee effect. Using both the discrete and continuum modelling tools we explore the complicated relationship between the long—term survival or extinction of the population and the initial spatial arrangement of the population. In particular, we study three different types of initial conditions: (i) a zero—dimensional initial condition where the initial density is independent of position in the domain; (ii) a one—dimensional initial condition where the initial density is independent of vertical position in the domain; and, (iii) a two—dimensional initial condition. Our results highlight the often—overlooked role of dimensionality in determining the long—term survival or extinction of bistable populations. These results are significant since we show that populations of individuals subjected to identical stochastic rules can either lead to survival or extinction as a result of differences in the initial spatial arrangement of the population. All software required to solve the stochastic and continuum models used in this work are available on GitHub

Keywords: population dynamics, birth, death, movement, reaction—diffusion, survival

1. Introduction

The classical logistic growth model is widely adopted in mathematical biology and mathematical ecology (Kot 2001; Murray 2002; Edelstein-Keshet 2005). In the logistic model, small initial population densities increase over time to approach a maximum carrying–capacity density (Maini et al. 2004a,b). An implicit assumption in using the logistic growth model is that any population, no matter how small, will always grow and survive. To address this limitation, more complicated models have been developed, including models based on the strong Allee effect (Allee and Bowen 1932; Lewis and Kareiva 1993; Stephens et al. 1999; Courchamp et al. 1999; Taylor and Hastings 2005; Courchamp et al. 2008; Arroyo-Esquivel and Hastings 2020). In the strong Allee model, initial densities greater than a threshold, called the *Allee threshold*, grow to eventually reach the carrying capacity, whereas initial densities less than the Allee threshold eventually go extinct (Allee and Bowen 1932; Courchamp et al. 1999; Taylor and Hastings 2005; Courchamp et al. 2008; Fadai and Simpson 2020). This kind of population dynamics, also referred to as a *bistable* population dynamics (Kot 2001), is often used to model situations where the potential for population extinction is thought to be important (Saltz and Rubenstein 1995; Courchamp et al. 1999; Drake 2004; Böttger et al. 2015; Vortkamp et al. 2020). In standard applications of bistable population dynamics, we often consider a mathematical model that takes the form of an ordinary differential equation (ODE). In this case, the eventual extinction or survival of the population is dictated solely by whether the initial density is greater than, or less than, the Allee threshold density. Such ODE models assume that the population is well–mixed, and hence neglects spatial effects. Spatial effects, such as moving invasion fronts, can be incorporated considering partial differential equations (PDEs) where the density of individuals depends explicitly upon position and time (Lewis and Kareiva 1993; Hastings et al. 2005). A common PDE framework is to consider a reaction–diffusion PDE with a cubic bistable source term (Neufeld et al. 2017; Johnston et al. 2017)

In this work we develop a mathematical modelling framework for studying bistable population dynamics on two–dimensional domains with periodic boundary conditions. Using this framework we explore how different initial densities and different initial spatial distributions of individuals influence the eventual survival or extinction of the population. Our modelling framework is based on a two–dimensional stochastic random walk model on a hexagonal lattice (Jin et al. 2016; Fadai et al. 2020). The stochastic model is an exclusion process, so

that each lattice site can be occupied by no more than one agent. Individuals in the model undergo a birth–death process that is modulated by local crowding effects (Jin et al. 2016; Johnston et al. 2017). The continuum limit of the stochastic model leads to a two–dimensional reaction–diffusion equation (RDE) with a bistable source term. This framework allows us to explore stochastic simulations together with solutions of the RDE. This approach is convenient because the stochastic model is more realistic in the sense that it incorporates fluctuations, but this benefit incurs additional computational overhead (Macfarlane et al. 2018; Chaplain et al. 2020). In contrast, the continuum limit RDE model can be solved very efficiently, but does not provide any information about the role of stochasticity (Macfarlane et al. 2018; Chaplain et al. 2020).

In all cases we study population dynamics on a square domain of side length L , with periodic boundary conditions along all boundaries. We explore the role of dimensionality by considering three different initial conditions. For the two–dimensional initial condition we distribute agents uniformly within a rectangle region of area $w_1 \times w_2$, as shown in Figure 1(a). For the one–dimensional initial condition we distribute agents uniformly within a column of width w_1 , as shown in Figure 1(b). For the zero–dimensional initial condition we distribute agents uniformly across the entire domain, as shown in Figure 1(c). Using both the discrete and continuum models we study the population dynamics associated with these three initial conditions, showing that the question of whether the population survives or goes extinct is more subtle than simply considering whether the initial density is above or below the Allee threshold. In fact, we observe different outcomes in terms of population extinction or survival depending on the dimensionality of the initial condition alone.

This work is organised as follows. In Section 2 we describe the stochastic individual–based model, paying particular attention to incorporating realistic movement and growth mechanisms. For simplicity, we use the generic term *growth* to indicate the birth/death process in the stochastic model. The reasons why we make a distinction between growth, and birth/death will become clear when we describe the modelling framework. In Section 3 we explain how to analyse the stochastic model using a mean–field assumption to arrive at an approximate continuum limit descriptions in terms of a classical RDE. Results in Section 4 show how both the stochastic and continuum models can be used to study the role of dimensionality by considering the three different initial conditions in Figure 1. The main results, in Section 5, systematically explore how population survival or extinction depends upon the dimensionality

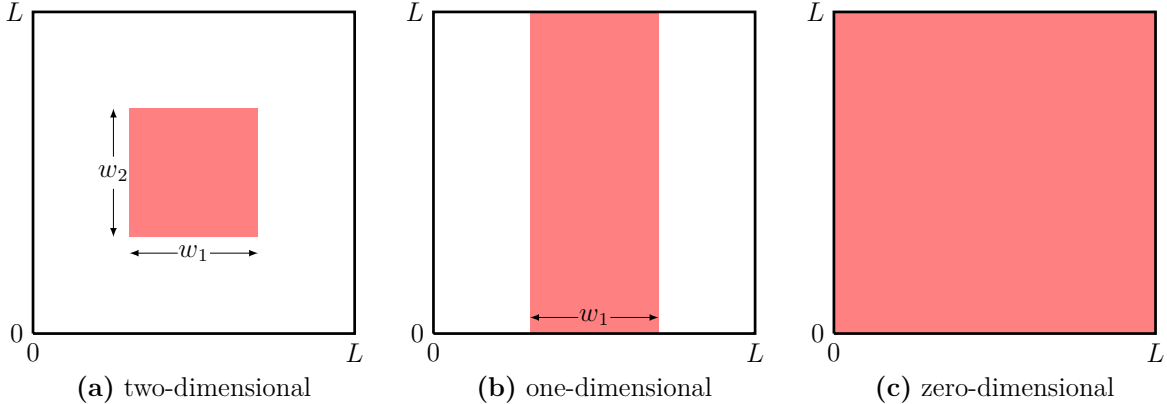


Figure 1: **Initial distributions with different dimensions on an $L \times L$ square domain.** In (a), individuals are distributed uniformly in the middle shaded square region, with length w_1 and width w_2 . In (b), individuals are distributed uniformly in a vertical strip of width w_1 , and height L . In (c), individuals are distributed uniformly in the $L \times L$ square domain.

of the problem. All software required to solve the stochastic and continuum models used in this work are available on GitHub

2. Discrete model

We consider a lattice-based discrete model describing movement, birth and death events in a population of individuals on a hexagonal lattice, with lattice spacing $\Delta > 0$. Each lattice site is indexed (i, j) , and has a unique Cartesian coordinate,

$$(x, y) = \begin{cases} \left(i\Delta, j\frac{\Delta\sqrt{3}}{2} \right), & \text{if } j \text{ is even,} \\ \left(\left(i + \frac{1}{2} \right) \Delta, j\frac{\Delta\sqrt{3}}{2} \right), & \text{if } j \text{ is odd.} \end{cases} \quad (1)$$

In any single realisation of the stochastic model site \mathbf{s} is either occupied, $C_{\mathbf{s}} = 1$, or vacant, $C_{\mathbf{s}} = 0$. If there are $Q(t)$ agents on the lattice at time t , we advance the stochastic simulation from time t to time $t + \tau$ by randomly selecting $Q(t)$ agents, with replacement, and allowing those agents to *attempt* to move. Once the $Q(t)$ potential movement events have been assessed, we then select $Q(t)$ agents at random, with replacement, to *attempt* to undergo a growth event, which could be either a birth or death event depending upon the local crowding conditions.

We now explain some features of the discrete model in terms of the schematic in Figure 2. In this initial description of the stochastic model we consider nearest neighbour movement and growth events only, and we will relax this assumption later. Figure 2(a) shows a potential

Movement probability: $\widehat{M}(K_s^{(m)}) = MG(K_s^{(m)})$

Birth/Death probability: $\widehat{P}(K_s^{(g)}) = P|F(K_s^{(g)})|$

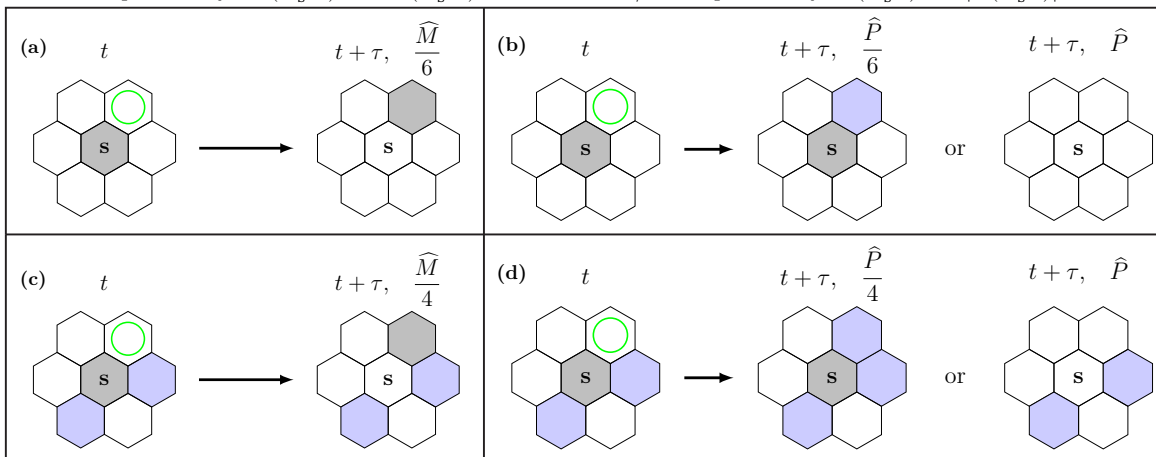


Figure 2: **Movement and growth mechanisms.** In each lattice fragment site s is shaded in grey, and occupied neighbouring sites are shaded in blue, while vacant neighbouring sites are unshaded (white). In (a) the agent at site s moves with probability \widehat{M} and moves to the target site, highlighted with a green circle, with probability $\widehat{M}/6$. In (b) the agent at site s undergoes a birth event with probability \widehat{P} and places a new agent on the target site with probability $\widehat{P}/6$ if the growth crowding function $F > 0$. In contrast, it dies with probability \widehat{P} if $F < 0$. In (c) the agent moves with probability \widehat{M} and moves to the target site with probability $\widehat{M}/4$. In (d) the agent undergoes a birth event with probability \widehat{P} and places a new agent on the target site with probability $\widehat{P}/4$ if $F > 0$. In contrast, it dies with probability \widehat{P} if $F < 0$.

movement event for an agent at site s , where all nearest neighbour sites are vacant. In this case, the probability of attempting to move during the next time step of duration τ , is $M \in [0, 1]$, and the attempted motility event will be successful with probability $\widehat{M} \leq M$. Here we note that the two probabilities, M and \widehat{M} are, in general, different. This difference is a result of the local crowding effects. The special case in Figure 2(a) where the agent at site s is uncrowded we have $\widehat{M} = M$. If the attempted motility event is successful, the agent at site s moves to a randomly-chosen vacant site chosen among the set of vacant nearest neighbour sites. In this case, as all six neighbour sites are vacant, the probability of moving to the target site, highlighted with a green circle, is $\widehat{M}/6$.

In Figure 2(b) we show a potential growth event for an agent at site s , where again all nearest neighbour sites are vacant. Here, the probability of attempting to grow in the next time step of duration τ is $P \in [0, 1]$, and the attempted growth event is successful with probability $\widehat{P} \leq P$. Again, the difference between P and \widehat{P} is caused by local crowding, and since this agent is uncrowded in this instance we have $\widehat{P} = P$. If the attempted growth event is successful, there are two possible outcomes. First, the growth event is a birth event. In this case a daughter agent is placed at a randomly-chosen vacant site within the set of nearest

neighbour sites with probability \widehat{P} . As there are six vacant neighbour sites, the probability of placing a daughter agent at the target site, highlighted in green, is $\widehat{P}/6$. Second, the growth event is a death event, and the agent is removed from the lattice, with probability \widehat{P} . The distinction between the birth and death events is governed by the sign of the growth crowding function, F , that will explain later.

To illustrate how crowding effects are incorporated into the movement component of the model, we now consider the schematic in Figure 2(c), where the agent at site \mathbf{s} is surrounded by two agents, highlighted in purple. The probability of attempting to move is $M \in [0, 1]$, and the attempted movement event is successful with probability $\widehat{M} = MG(K_{\mathbf{s}}^{(m)})$. Here, $K_{\mathbf{s}}^{(m)}$ is a measure of the local density of site \mathbf{s} and we call $G(K_{\mathbf{s}}^{(m)}) \in [0, 1]$ the *movement crowding function* that specifies how the local density influences potential movement events. In a successful movement event, as there are four vacant neighbour sites, the probability of moving to the target site, highlighted in green, is $\widehat{M}/4$.

Figure 2(d) illustrates how crowding effects are incorporated into the growth component of the model, where the agent at site \mathbf{s} is surrounded by two agents. The probability of attempting to grow is $P \in [0, 1]$, and the attempted growth is successful with probability $\widehat{P} = P|F(K_{\mathbf{s}}^{(g)})|$. Here, $K_{\mathbf{s}}^{(g)}$ is again a measure of the local density of site \mathbf{s} and the function $F(K_{\mathbf{s}}^{(g)}) \in [-1, 1]$ is called the *growth crowding function* that specifies how the local density influences the ability of this agent to undergo a growth event. If this attempt is successful, there are two possible outcomes reflected by the sign of F . If $F > 0$, the growth event is a birth event, and a daughter agent is placed at a randomly-chosen vacant site with probability \widehat{P} . As there are four vacant neighbour sites, the probability of placing a daughter agent at the vacant target site, highlighted in green, is $\widehat{P}/4$. Second, if $F < 0$, the growth event is a death event, and the agent is removed from the lattice. The special case where $F = 0$ leads to no change.

A key feature of our model is in the way that the local density about each site affects movement and growth events through the movement and growth crowding functions. To describe this we take $\mathcal{N}_r\{\mathbf{s}\}$ to denote the set of neighbouring sites around site \mathbf{s} , where $r \geq 1$ is the integer number of concentric rings of sites surrounding site \mathbf{s} (Jin et al. 2016; Fadai et al. 2020). Here, $|\mathcal{N}_r| = 3r(r + 1)$. The probability that any potential movement or growth event

is successful depends upon the local density about site \mathbf{s} ,

$$K_{\mathbf{s}}(r) = \frac{1}{|\mathcal{N}_r|} \sum_{\mathbf{s}' \in \mathcal{N}_r\{\mathbf{s}\}} C_{\mathbf{s}'}, \quad (2)$$

where $K_{\mathbf{s}}(r) \in [0, 1]$ is a simple measure of the crowdedness of the local region surrounding site \mathbf{s} . While in Figure 2 we explain the model with $r = 1$ and $|\mathcal{N}_1| = 6$, it is possible to use different sized templates, depending on the choice of r . Sometimes it is useful for us to use different sized templates for the movement and growth mechanisms. For example, Simpson et al. (2010) argue that cell migration can be modelled using a nearest-neighbour random walk with $r = 1$ to represent cell migration, whereas cell proliferation involves non nearest-neighbour interactions since daughter cells are often deposited several cell diameters away from the location of the mother cell. To simulate this they introduce proliferation mechanisms where daughter agents are placed up to four lattice sites away from the mother agent in order to faithfully represent the underlying biological detail into their model. This would be similar to setting $r = 1$ for movement and $r = 4$ for growth. Therefore, it is convenient for us to make a notational distinction between the size of the templates for motility and growth. Therefore, we denote the motility template as $K_{\mathbf{s}}^{(m)} = K_{\mathbf{s}}(r')$ and the growth template as $K_{\mathbf{s}}^{(g)} = K_{\mathbf{s}}(r'')$ where $r' \geq 1$ and $r'' \geq 1$ two, potentially different, positive integers.

We now describe the details of how crowding effects and different sized spatial templates are incorporated into the growth component of the model with reference to the schematic illustration in Figure 3. In Figure 3(a)–(c), crowding of the agent at site \mathbf{s} is measured using a nearest neighbour template with $r = 1$, and the growth crowding function given in Figure 3(d) such that the probability of undergoing a birth event is $\hat{P} = P|F(K_{\mathbf{s}}^{(g)})|$. In Figure 3(a) where $K_{\mathbf{s}}^{(g)} = 0$, we have $F(0) = 1$ and $\hat{P} = P$. As there are six vacant sites in \mathcal{N}_1 , the probability of placing a daughter agent at the target site, highlighted in green, is $\hat{P}/6$. In Figure 3(b) where the agent at site \mathbf{s} is surrounded by two neighbour agents, the probability of undergoing a birth event is $\hat{P} = 2P/3$, since $K_{\mathbf{s}}^{(g)} = 1/3$ and $F(1/3) = 2/3$. As there are four vacant sites in \mathcal{N}_1 , the probability of placing a daughter agent at the target site is $\hat{P}/4$. Similarly, in Figure 3(c), we have $\hat{P} = P/3$ as $K_{\mathbf{s}}^{(g)} = 2/3$ and $F(2/3) = 1/3$. As there are two vacant sites in \mathcal{N}_1 , the probability of placing a daughter agent at the target site is $\hat{P}/2$.

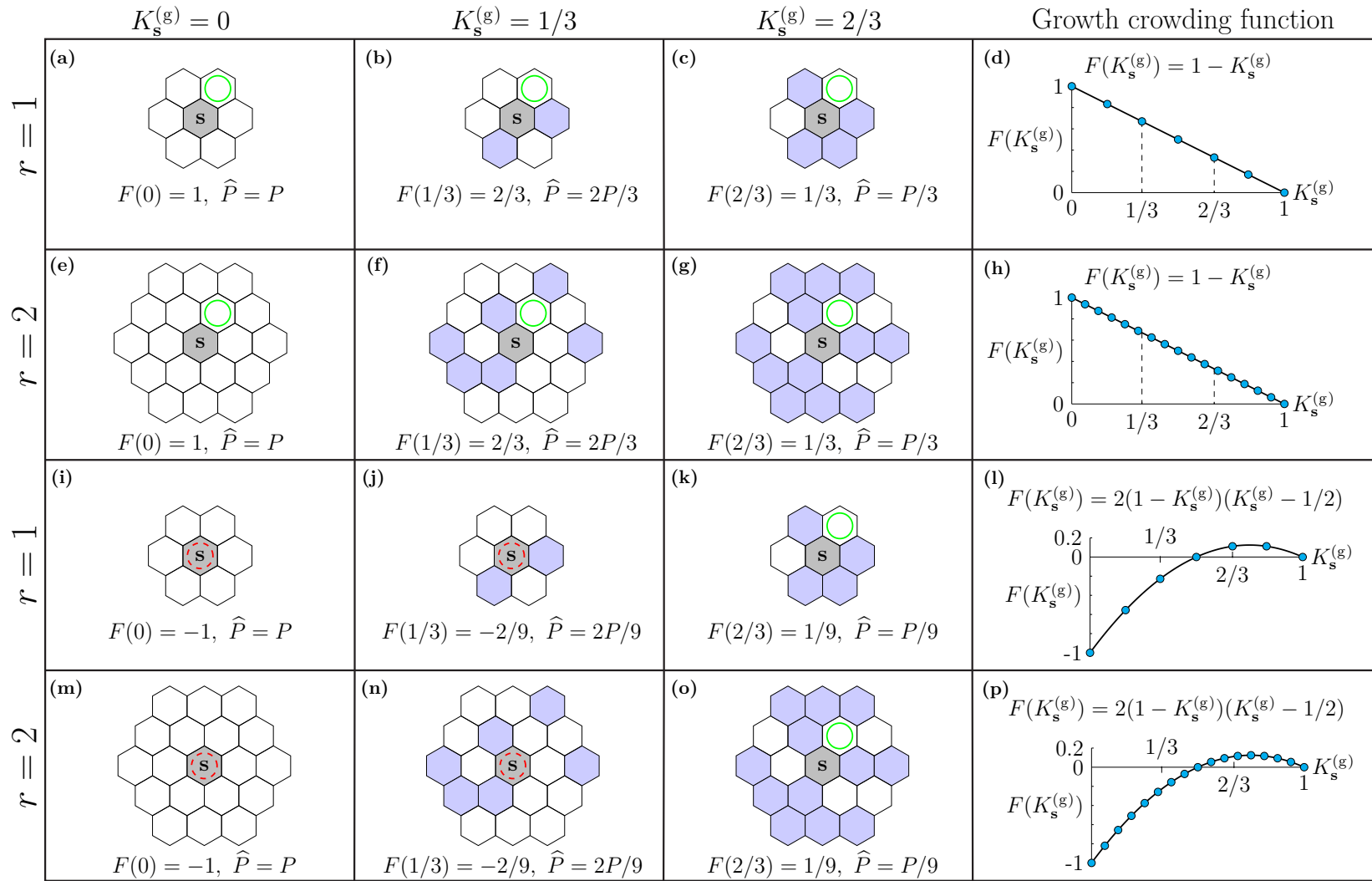


Figure 3: **Growth mechanisms with different sized spatial templates and growth crowding functions.** In each lattice fragment site s is shaded grey, occupied sites within the template are shaded blue, and vacant sites within the template are unshaded (white). Each subfigure shows a potential outcome for an agent at site s . With $r = 1$, the crowdedness of \mathcal{N}_1 is shown in (a)–(c) and (i)–(k). With $r = 2$, the crowdedness of \mathcal{N}_2 is shown in (e)–(g) and (m)–(o). The agent at site s can lead to a birth event when $F > 0$ as in (a)–(c), (e)–(g), (k) and (o). In contrast the agent at site s can lead to a death event when $F < 0$ as in (i), (j), (m) and (n). The solid green circles represent the target site for the placement of a daughter agent during a successful proliferation event, and the dashed red circles indicate the location of agents that can undergo a death event.

In Figure 3(e)–(g) we introduce a non nearest–neighbour growth mechanism by measuring the crowdedness of the agent at site \mathbf{s} using a larger spatial template with $r = 2$. Therefore, if the agent at \mathbf{s} undergoes a successful birth event, the daughter agent is able to be placed at any vacant site within \mathcal{N}_2 . The probability of undergoing a birth event is $\widehat{P} = PF(K_{\mathbf{s}}^{(g)})$. For the agent in Figure 3(e) where $K_{\mathbf{s}}^{(g)} = 0$ and $F(0) = 1$, we have $\widehat{P} = P$. In this configuration there are 18 vacant sites in \mathcal{N}_2 and the probability of placing a daughter agent at the target site, highlighted in green, is $\widehat{P}/18$. In Figure 3(f) where the agent at site \mathbf{s} is surrounded by six neighbour agents, the probability of undergoing a birth event is $\widehat{P} = 2P/3$, as $K_{\mathbf{s}}^{(g)} = 1/3$ and $F(1/3) = 2/3$. Since there are 12 vacant sites in \mathcal{N}_2 , the probability of placing a daughter agent at the target site is $\widehat{P}/12$. Similarly, in Figure 3(g), we have $\widehat{P} = P/3$, as $K_{\mathbf{s}}^{(g)} = 2/3$ and $F(2/3) = 1/3$. The probability of placing a daughter agent at the target site is $\widehat{P}/6$. All results in Figure 3(a)–(c) and Figure 3(e)–(g) consider the simplest linear crowding function $F(K_{\mathbf{s}}^{(g)}) = 1 - K_{\mathbf{s}}^{(g)}$, and we now explore other choices of $F(K_{\mathbf{s}}^{(g)})$.

We now choose a nonlinear growth crowding function $F(K_{\mathbf{s}}^{(g)})$ that can take on both positive and negative values, as shown in Figure 3(l). In this case we make a distinction between a birth event when $F(K_{\mathbf{s}}^{(g)}) > 0$, a death event when $F(K_{\mathbf{s}}^{(g)}) < 0$, and no event when $F(K_{\mathbf{s}}^{(g)}) = 0$. We first consider a nearest neighbour template with $r = 1$ in Figure 3(i)–(k). In Figure 3(i), the agent at site \mathbf{s} dies with probability $\widehat{P} = P|F(K_{\mathbf{s}}^{(g)})|$. Here, $K_{\mathbf{s}}^{(g)} = 0$ and $F(0) = -1$, thus $\widehat{P} = P$. In Figure 3(j) the agent at site \mathbf{s} dies with probability $\widehat{P} = 2P/9$ as $K_{\mathbf{s}}^{(g)} = 1/3$ and $F(1/3) = -2/9$. In Figure 3(k) the agent at site \mathbf{s} undergoes a birth event with probability $\widehat{P} = P/9$ as $K_{\mathbf{s}}^{(g)} = 2/3$ and $F(2/3) = 1/9$. As there are two vacant sites in \mathcal{N}_1 , the probability of placing a daughter agent at the target site is $\widehat{P}/2$.

Finally, we consider a larger template with \mathcal{N}_2 in Figure 3(m)–(o). In Figure 3(m), the agent at site \mathbf{s} dies with probability $\widehat{P} = P|F(K_{\mathbf{s}}^{(g)})|$. Here $K_{\mathbf{s}}^{(g)} = 0$ and $F(0) = -1$, thus $\widehat{P} = P$. In Figure 3(n), the agent at site \mathbf{s} dies with probability $\widehat{P} = 2P/9$ as $K_{\mathbf{s}}^{(g)} = 1/3$ and $F(1/3) = -2/9$. In Figure 3(o) the agent at site \mathbf{s} undergoes a birth event with probability $\widehat{P} = P/9$ as $K_{\mathbf{s}}^{(g)} = 2/3$ and $F(2/3) = 1/9$. As there are six vacant sites in \mathcal{N}_2 , the probability of placing a daughter agent at the target site is $\widehat{P}/6$.

The movement crowding function $G(K_{\mathbf{s}}^{(m)})$ works in a similar way as the growth crowding function $F(K_{\mathbf{s}}^{(g)})$, except that it is always positive, $G(K_{\mathbf{s}}^{(m)}) \in [0, 1]$. In this section we have sought to describe the discrete mechanism as clearly as possible with the use of Figure 2 and Figure 3. The pseudo-code for the stochastic model is given in Appendix A. For the remainder

of this work we focus on results where we set $r = 1$ for movement and $r = 4$ for growth. This choice is motivated by experimental images of cell proliferation where careful examination of timelapse movies show that daughter cells are often placed some distance from the mother cell (Simpson et al. 2010). Other choices of r can be implemented using the software available on GitHub

3. Continuum limit

In this section we derive the mean-field continuum limit of the discrete model. The *averaged* occupancy of site \mathbf{s} , constructed from V identically-prepared realisations of the discrete model, can be written as

$$\bar{C}_{\mathbf{s}} = \frac{1}{V} \sum_{v=1}^V C_{\mathbf{s}}^{(v)}(t), \quad (3)$$

where $C_{\mathbf{s}}^{(v)}(t) \in \{0, 1\}$ is the binary occupancy of site \mathbf{s} at time t in the v th identically-prepared realisation of the discrete model, and $C_{\mathbf{s}} \in [0, 1]$ is the smooth averaged occupancy. We note that $\bar{C}_{\mathbf{s}}$ is a function of time, t , but we suppress this dependence for notational convenience. Similarly, the *averaged* occupancy of $\mathcal{N}_r\{\mathbf{s}\}$, again constructed from V identically-prepared realisations, is given by

$$\bar{K}_{\mathbf{s}}(r) = \frac{1}{|\mathcal{N}_r|} \sum_{\mathbf{s}' \in \mathcal{N}_r\{\mathbf{s}\}} \bar{C}_{\mathbf{s}'}. \quad (4)$$

As we use a nearest neighbour template, $r = 1$, for movement, and a larger template, $r = 4$, for growth, we denote the averaged occupancy of sites for potential movement events as $\bar{K}_{\mathbf{s}}^{(m)}$, and the averaged occupancy of sites for potential growth events as $\bar{K}_{\mathbf{s}}^{(g)}$.

To arrive at an approximate continuum limit description, we start by writing down an expression for the expected change in occupancy of site \mathbf{s} during the time interval from t to $t + \tau$,

$$\begin{aligned} \delta(C_{\mathbf{s}}) = & \overbrace{\frac{M}{|\mathcal{N}_1|} (1 - \bar{C}_{\mathbf{s}}) \sum_{\mathbf{s}' \in \mathcal{N}_1\{\mathbf{s}\}} \bar{C}_{\mathbf{s}'} \frac{G(\bar{K}_{\mathbf{s}'}^{(m)})}{1 - \bar{K}_{\mathbf{s}'}^{(m)}}}_{\text{move into } \mathbf{s}} - \overbrace{M \bar{C}_{\mathbf{s}} G(\bar{K}_{\mathbf{s}}^{(m)})}_{\text{move out of } \mathbf{s}} \\ & + \underbrace{\frac{P}{|\mathcal{N}_4|} (1 - \bar{C}_{\mathbf{s}}) \sum_{\mathbf{s}' \in \mathcal{N}_4\{\mathbf{s}\}} \mathbb{H}(F(\bar{K}_{\mathbf{s}'}^{(g)})) \bar{C}_{\mathbf{s}'} \frac{F(\bar{K}_{\mathbf{s}'}^{(g)})}{1 - \bar{K}_{\mathbf{s}'}^{(g)}}}_{\text{birth events: place new agents onto } \mathbf{s}} \\ & - \underbrace{(1 - \mathbb{H}(F(\bar{K}_{\mathbf{s}}^{(g)}))) P \bar{C}_{\mathbf{s}} F(\bar{K}_{\mathbf{s}}^{(g)})}_{\text{death event: remove agent from } \mathbf{s}}, \end{aligned} \quad (5)$$

where \mathbb{H} is the Heaviside step function. Each term in Equation (5) has a relatively simple physical interpretation. The first term on the right hand side of Equation (5) represents the change in occupancy of site \mathbf{s} owing to the expected movement of agents in $\mathcal{N}_1\{\mathbf{s}\}$ into site \mathbf{s} . The factor $1/(1 - \bar{K}_{\mathbf{s}}^{(m)})$ accounts for the choice of the target site in \mathcal{N}_1 being randomly selected from the available vacant sites. The second term on the right hand side of Equation (5) represents the change in occupancy of site \mathbf{s} owing to the expected movement of agents out of site \mathbf{s} . The third term on the right hand side of Equation (5) represents the change in occupancy owing to the expected birth events of agents in $\mathcal{N}_4\{\mathbf{s}\}$ that would place daughter agents onto site \mathbf{s} , where $F(\bar{K}_{\mathbf{s}}^{(g)}) > 0$. Again, the factor $1/(1 - \bar{K}_{\mathbf{s}}^{(g)})$ accounts for the choice of the target site in \mathcal{N}_4 being randomly selected from the available vacant sites. The last term on the right hand side of Equation (5) represents the expected change in occupancy owing to agent death at site \mathbf{s} , when $F(\bar{K}_{\mathbf{s}}^{(g)}) < 0$. Note that this approximate conservation statement makes use of the mean-field assumption, whereby the occupancy status of lattice sites are taken to be independent (Baker and Simpson 2010).

To derive the continuum limit we identify $\bar{C}_{\mathbf{s}}$ with a continuous function $C(x, y, t)$ and then expand each term in Equation (5) in a truncated Taylor series about site \mathbf{s} where we ignore terms $\mathcal{O}(\Delta^3)$ and smaller. Subsequently, we divide both sides by τ and evaluate the resulting expressions in the limit $\Delta \rightarrow 0$ and $\tau \rightarrow 0$ jointly, with the ratio of Δ^2/τ held constant (Hughes 1995). This leads to the following nonlinear RDE,

$$\frac{\partial C(x, y, t)}{\partial t} = D_0 \nabla \cdot (D(C) \nabla C(x, y, t)) + \lambda C(x, y, t) F(C), \quad (6)$$

where

$$D(C) = C \frac{dG(C)}{dC} + \frac{1+C}{1-C} G(C), \quad (7)$$

and

$$D_0 = \frac{M}{4} \lim_{\Delta, \tau \rightarrow 0} \frac{\Delta^2}{\tau}, \quad \lambda = \lim_{\tau \rightarrow 0} \frac{P}{\tau}. \quad (8)$$

Here, D_0 is the free-agent diffusivity, $D(C)$ is a nonlinear diffusivity function, and λ is the rate coefficient associated with the source term. To obtain a well-defined continuum limit we require that $P = \mathcal{O}(\tau)$ (Simpson et al. 2010). The algebraic details required to arrive at the continuum limit are outlined, in detail, in Appendix B.

For all simulations in this work we use $\Delta = \tau = 1$, which is equivalent to working in a

non-dimensional framework (Simpson et al. 2010). If the model is to be applied to a particular dimensional problem, then Δ and τ can be re-scaled appropriately. In this non-dimensional framework we satisfy the requirement that $P = \mathcal{O}(\tau)$ by setting $P \ll M$. The focus of this work is on the role of the growth mechanism, and the question of whether the population survives or goes extinct, we set $G(C) = 1 - C$, leading to $D(C) = 1$. This means that the nonlinear diffusion term in Equation (6) simplifies to a linear diffusion term, giving

$$\frac{\partial C(x, y, t)}{\partial t} = D_0 \nabla^2 C(x, y, t) + \lambda C(x, y, t) F(C). \quad (9)$$

We note that Equation (9) has been studied extensively in applications involving the spatial spread of invasive species (Fisher 1937; Skellam 1951; Fife 1979; Lewis and Kareiva 1993; Hastings et al. 2005). Some of these models of invasion consider a logistic-type source term (Fisher 1937; Perumpanani et al. 1999), while others consider Allee-type bistable source term (Fife 1979; Lewis and Kareiva 1993; Sewalt et al. 2016). Under these conditions many results have been established. For example, if we consider (9) on a one-dimensional infinite domain, it is well known that this model supports travelling wave solutions for both logistic (Fisher 1937) and bistable (Fife 1979) source terms. In this work, however, we take a different perspective by studying Equation (9) on a finite domain and so the question of analysing travelling wave solutions is our focus.

In the rest of this work we choose on

$$F(C) = a(1 - C)(C - A), \quad (10)$$

since this leads to the canonical cubic source term $\lambda C F(C)$ associated with Allee kinetics. In particular, we set $a = 5/2$ and $A = 2/5$ so that this choice of $F(C)$ can be used to represent both birth and death events in a simple way. This choice of parameters gives $F(0) = -1$ so that attempted death events for an isolated agent where $C = 0$ is always successful.

In summary, our discrete model requires the specification of two crowding functions: $G(C)$, the crowding function for movement events, and $F(C)$, the crowding function for growth events. These microscopic crowding functions are related to macroscopic quantities in the associated RDE model. In particular, $G(C)$ is related to a nonlinear diffusivity function, $D(C)$, and $F(C)$ is related to a nonlinear source term $\lambda C F(C)$. Profiles in Figure 4 show the relationship between these functions for our choice of $G(C)$ and $F(C)$. Note that our special

choice of $G(C) = 1 - C$ leads to a linear diffusion model where $D(C) = 1$.

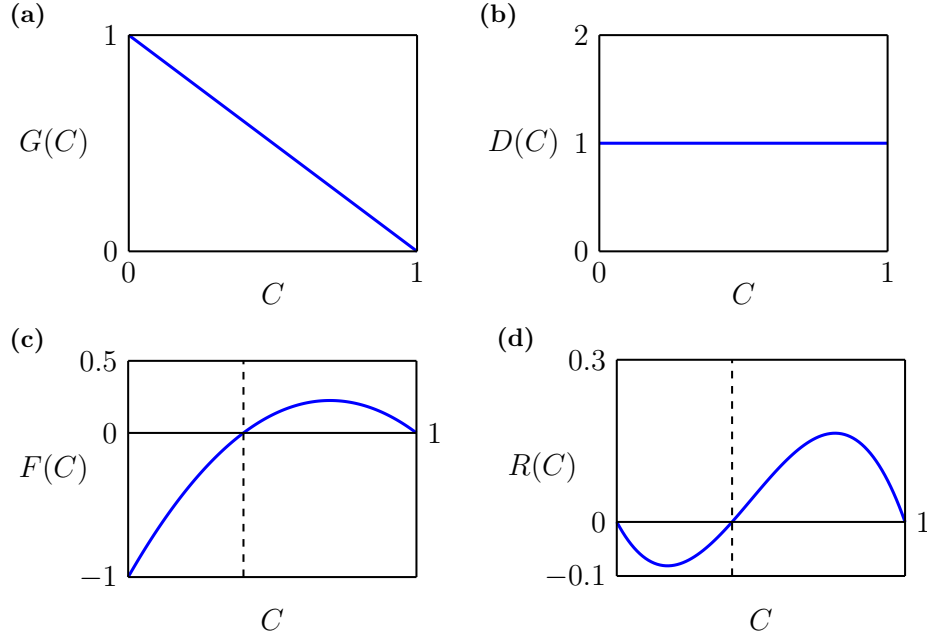


Figure 4: **Specific crowding functions used in this work.** (a)–(b) Setting $G(C) = 1 - C$ for the motility crowding function leads to linear diffusion, $D(C) = 1$. (c)–(d) Setting $F(C) = 2.5(1 - C)(C - 0.4)$ for the growth crowding function leads to $\lambda C F(C) = 2.5C(1 - C)(C - 0.4)$. The dashed lines in (c)–(d) relate to the Allee threshold, $A = 0.4$.

4. Initial conditions and simulation data

In this section we consider the three initial conditions shown in Figure 1, and we introduce the corresponding continuous descriptions. In general, each of the initial conditions shown in Figure 1 can be written as

$$C(x, y, 0) = \begin{cases} B, & (x, y) \in \mathcal{H}, \\ 0, & \text{elsewhere,} \end{cases} \quad (11)$$

where \mathcal{H} is the region in which individuals are uniformly distributed at density $B \in (0, 1]$. The key difference between the three initial conditions in Figure 1 is the shape of the region \mathcal{H} .

For the three initial conditions in Figure 1 we will report data from the stochastic model in the following way. For simulations relating to the two-dimensional initial conditions as in Figure 1(a) we denote the averaged occupancy of site \mathbf{s} as

$$\langle C(x, y, t) \rangle = \frac{1}{V} \sum_{v=1}^V C^{(v)}(i, j, n), \quad (12)$$

where we note that the lattice indices i and j are related to position, (x, y) , via Equation (1). Here, $\langle C(x, y, t) \rangle$ is a measure of the local density at location (x, y) , and time $t = n\tau$ after the n th time step in the discrete stochastic model. The average is constructed using V identically-prepared realisations of the stochastic model. Similarly, for simulations relating to the one-dimensional initial conditions as in Figure 1(b), where the initial occupancy is independent of the vertical position, we denote the averaged occupancy of any site as

$$\langle C(x, t) \rangle = \frac{1}{VJ} \sum_{v=1}^V \sum_{j=1}^J C^{(v)}(i, j, n), \quad (13)$$

which is a measure of the density at location x and at time $t = n\tau$. Note that, as we will show through simulation, the density of agents remains independent of vertical position for all $t > 0$ because we use periodic boundary conditions. For simulations relating to the zero-dimensional initial conditions as in Figure 1(c), where the initial density is independent of position, we denote the averaged occupancy of any site as

$$\langle C(t) \rangle = \frac{1}{VIJ} \sum_{v=1}^V \sum_{j=1}^J \sum_{i=1}^I C^{(v)}(i, j, n), \quad (14)$$

which is a measure of the total population density at time $t = n\tau$. Again, as we will show through simulation, the density of agents remains independent of position for all $t > 0$. In this work the averaged occupancy $\langle C(t) \rangle$ is also useful to describe simulations starting from the two-dimensional and one-dimensional initial conditions. In summary, data from the discrete models includes $\langle C(x, y, t) \rangle$, $\langle C(x, t) \rangle$, and $\langle C(t) \rangle$.

To compare averaged data from the discrete model with the solution of the continuum model we solve Equation (9) numerically to give $C(x, y, t)$. Full details of the numerical methods are outlined in the Appendix C. Using the numerical solution for $C(x, y, t)$ calculate

$$\mathcal{C}(t) = \frac{1}{L^2} \int_0^L \int_0^L C(x, y, t) dx dy,$$

which is a measure of the density of the population across the entire $L \times L$ domain.

Results in Figure 5 compare data from the discrete model with numerical solutions of the continuum model for the two-dimensional initial condition. The initial condition in Figure 5(a) shows a square region, of size 40×40 that is occupied with density $B = 1$. Simulations are performed with $M = 1$ and $P = 1/1000$, leading to $D_0 = 1/4$ and $\lambda = 1/1000$. Figure 5(b)

shows a snapshot from the discrete model at $T = \lambda t = 0.5$ where we see the agents spreading into the domain. The numerical solution of Equation (9) in Figure 5(c) shows the solution of the continuum limit RDE at $T = 0.5$. The visual comparison between the spatial arrangement and density of the profiles in Figure 5(b) and Figure 5(c) appears to be very good, with the solution of the continuum model appearing to capture the key features of the discrete simulation. To make a more quantitative comparison we examine the density along the horizontal dashed lines shown in Figures 5(b)–(c) at $y = 50$. Figure 5(d) compares the evolution of $C(x, 50, T)$ and $\langle C(x, 50, T) \rangle$, and we see that the match between the solution of the continuum model and appropriately averaged data from the discrete model is excellent. Finally, in Figure 5(e) we compare the averaged total occupancy from the discrete model, $\langle C(T) \rangle$, with $\mathcal{C}(T)$ from the solution of the continuum model. Again, we see that the discrete–continuum comparison is excellent, and that the continuum model predicts the eventual extinction of this population. This is an interesting result given that the initial density in the centre of the domain is greater than the Allee threshold, yet the total population eventually becomes extinct.

We now consider a second set of discrete–continuum comparisons for precisely the same mechanisms except that the spatial arrangement of the initial condition, shown in Figure 5(f) is larger and occupying the central 80×80 region of the domain. A snapshot from a typical discrete simulation in Figure 5(g) appears to compare well with the numerical solution of the continuum model in Figure 5(h). A more quantitative comparison of the evolution of $C(x, 50, T)$ and $\langle C(x, 50, T) \rangle$ in Figure 5(i) confirms the accuracy of the continuum model. Figure 5(j) compares $\langle C(T) \rangle$ and $\mathcal{C}(T)$, where we see that the population eventually grows to reach the maximum density.

Overall, the results in Figure 5 confirm that the numerical solution of the continuum model, Equation (9), can provide an accurate way of studying the expected behaviour of the discrete model. We are interested in the long–term outcomes of precisely the same discrete mechanism in Figure 5(a)–(e) and Figure 5(f)–(j), where the population eventually becomes extinct in the former case, while surviving in the latter case. The only difference is in the spatial arrangement of the initial condition.

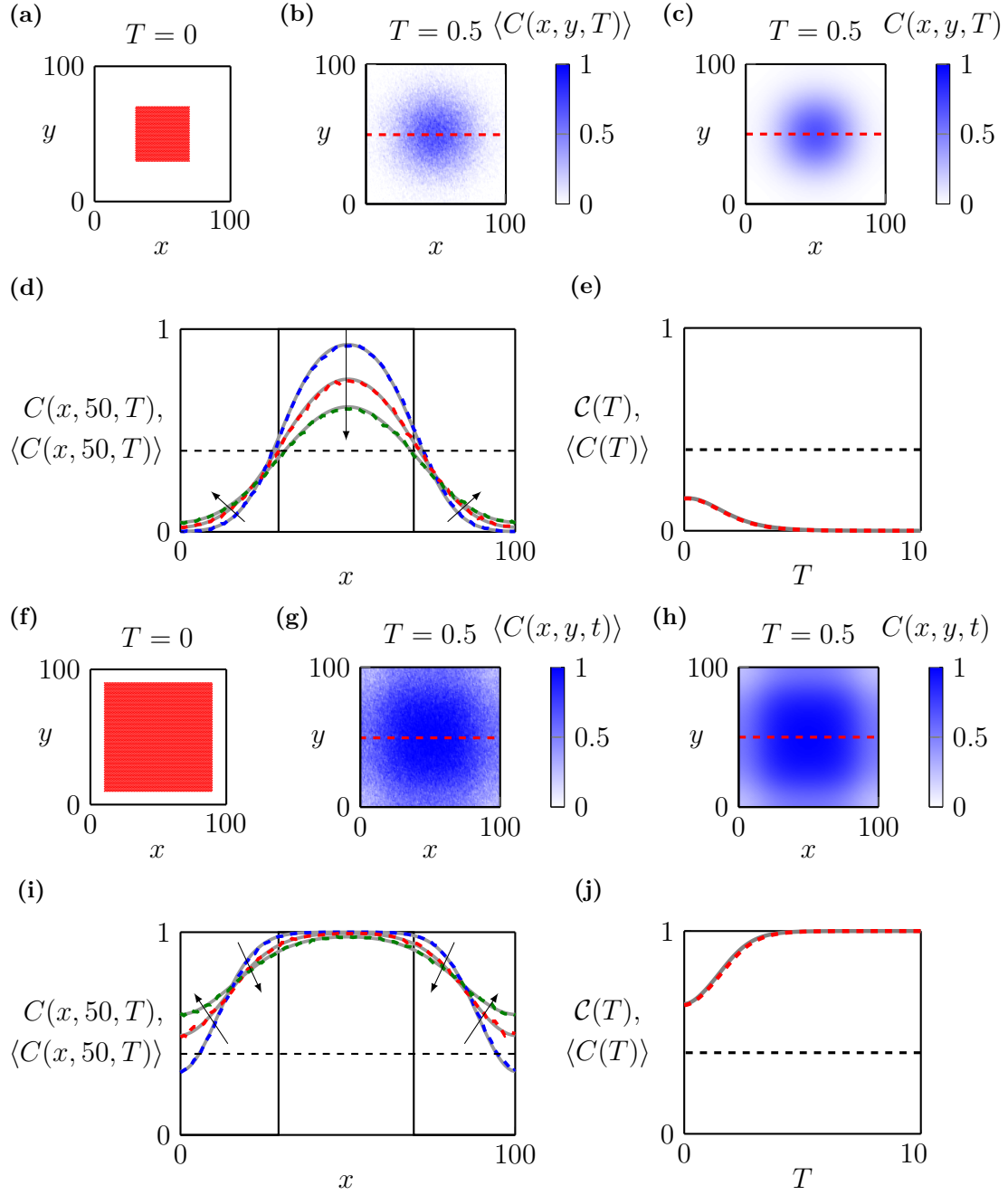


Figure 5: **Comparison of data from the discrete model with the solution of the continuum model for the two-dimensional initial condition.** In (a) agents are initially located in a square region of size 40×40 with $B = 1$. (b) $\langle C(x, y, T) \rangle$ at $T = \lambda t = 0.5$. (c) $C(x, y, T)$ at $T = \lambda t = 0.5$. (d) $\langle C(x, 50, T) \rangle$ (dashed) and $C(x, 50, T)$ (solid) at $T = 0.2, 0.4, 0.6$. (e) $\langle C(T) \rangle$ (dashed red) and $C(T)$ (solid grey). In (f) agents are initially located at a square region of size 80×80 with $B = 1$. (g) $\langle C(x, y, t) \rangle$ at $T = \lambda t = 0.5$. (h) $C(x, y, t)$ at time $T = \lambda t = 0.5$. (i) $\langle C(x, 50, T) \rangle$ (dashed) and $C(x, 50, T)$ (solid) at $T = 0.2, 0.4, 0.6$. (j) $\langle C(T) \rangle$ (dashed red) and $C(T)$ (solid grey). The dashed black horizontal lines in (d), (e), (i) and (j) indicate the Allee threshold, $A = 0.4$. Arrows in (d) and (i) show the direction of increasing time. Note that we generate 40 identically-prepared realisations to obtain $\langle C(x, y, T) \rangle$ in (b) and (g), 40 identically-prepared realisations to obtain $\langle C(T) \rangle$ in (e) and (j), and 4000 identically-prepared realisations to obtain $\langle C(x, 50, T) \rangle$ in (d) and (i). All discrete simulations correspond to $M = 1$ and $P = 1/1000$.

For the one-dimensional initial condition, as shown in Figure 1(b), Equation (9) simplifies to

$$\frac{\partial C(x, t)}{\partial t} = D_0 \frac{\partial^2 C(x, t)}{\partial x^2} + \lambda C(x, t) F(C), \quad (15)$$

where $C(x, t)$ represents the column-averaged density of agents (Simpson et al. 2010). An extensive discussion and exploration about the implications of simplifying the two-dimensional nonlinear RDE into this simpler one-dimensional RDE is given in Simpson (2009). Given a numerical solution of Equation (15), as outlined in Appendix C, we compute

$$\mathcal{C}(t) = \frac{1}{L} \int_0^L C(x, t) dx,$$

which, again, is a measure of the density of the population across the entire $L \times L$ domain.

Results in Figure 6 give a comparison between the discrete and continuum solutions for the one-dimensional initial condition. The initial condition in Figure 6(a) shows that the central strip of width 16 is occupied with density $B = 1$. Figures 6(b)–(c) show snapshots from the discrete model as the population spreads into the domain. Figure 6(d) compares the numerical solution of Equation (15), $C(x, T)$, with averaged data from the discrete model, $\langle C(x, T) \rangle$. The evolution of the total population density in the discrete model, $\langle C(T) \rangle$, and in the continuum model, $\mathcal{C}(T)$, is compared in Figure 6(e). In all cases the continuum model accurately captures the averaged data from the discrete model, and in this case the population eventually becomes extinct. Again, this is an interesting result because the initial density of agents in the central vertical strip exceeds the Allee threshold.

We then consider a second set of discrete-continuum comparisons for precisely the same mechanisms except that the spatial arrangement of the initial condition, shown in Figure 6(f), is larger and occupying the central vertical strip of width 64 with density $B = 1$. Figures 6(g)–(h) show discrete snapshots as the population spreads. The comparisons between $C(x, T)$ and $\langle C(x, T) \rangle$ in Figure 6(i), and between $\mathcal{C}(T)$ and $\langle C(T) \rangle$ in Figure 6(j) are excellent. In this case we see that the population eventually grows to reach the maximum density. For the one-dimensional initial condition it is interesting to note that the long-term outcomes of precisely the same discrete mechanism in Figure 6(a)–(e) and Figure 6(f)–(j), leads to very different outcomes, where the population eventually becomes extinct in the former case, while surviving in the latter case. The only difference is in the width of the initial population.

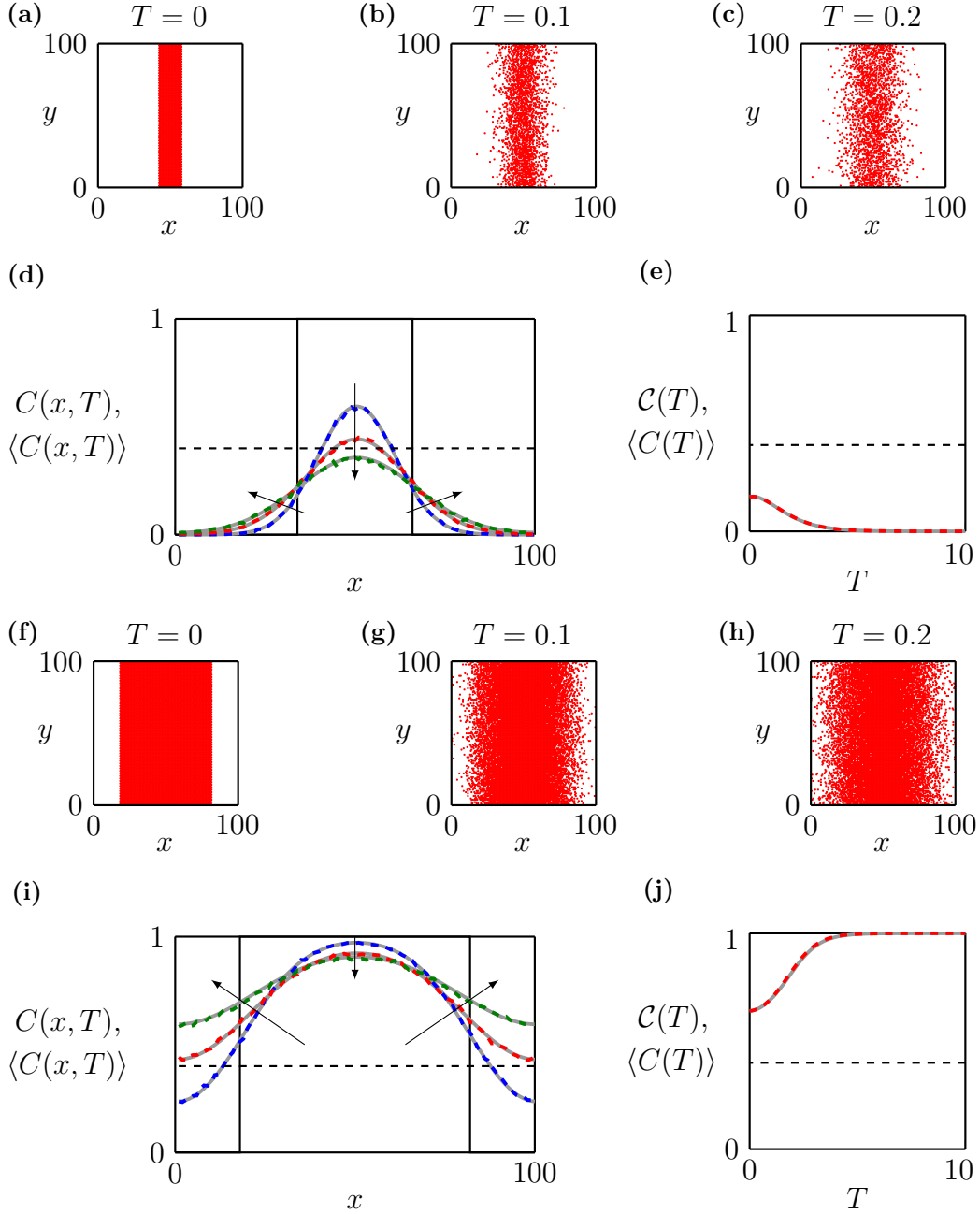


Figure 6: **Comparison of data from the discrete model with the solution of the continuum model for the one-dimensional initial condition.** In (a), agents are initially placed within a vertical strip where $x \in [42, 58]$, with $B = 1$. (b)–(c) snapshots from the discrete model at $T = 0.1$ and $T = 0.2$, respectively. (d) $\langle C(x, T) \rangle$ (dashed) and $C(x, T)$ (solid) at time $T = 0.2, 0.4, 0.6$. (e) $\langle C(t) \rangle$ (dashed red) and $C(t)$ (solid grey). In (f), agents are initially placed within a vertical strip where $x \in [16, 84]$, with $B = 1$. (g)–(h) snapshots from the discrete model at $T = 0.1$ and $T = 0.2$, respectively. (i) $\langle C(x, T) \rangle$ (dashed) and $C(x, T)$ (solid) at time $T = 0.2, 0.4, 0.6$. (j) $\langle C(t) \rangle$ (red dashed) and $C(t)$ (grey solid). The dashed black horizontal lines in (d), (e), (i) and (j) indicate the Allee threshold, $A = 0.4$. Arrows in (d) and (i) show the direction of increasing time. Note that we generate 40 identically-prepared realisations to obtain $\langle C(x, T) \rangle$ in (d) and (i), and also 40 identically-prepared realisations to obtain $\langle C(T) \rangle$ in (e) and (j).

For the zero-dimensional initial condition, as shown in Figure 1(c), Equation (9) simplifies to

$$\frac{dC(t)}{dt} = \lambda C(t)F(C), \quad (16)$$

where $C(t)$ represents the total density of agents. With our choice of Allee kinetics, this ODE can be solved to give an implicit solution. Results in Figure 7 compare the discrete and continuum solutions for the zero-dimensional initial condition. In Figure 7(a), a fixed number of agents are randomly distributed in the entire domain leading to $\langle C(0) \rangle = 0.16$. Figures 7(b)–(c) show discrete snapshots as the population evolves.

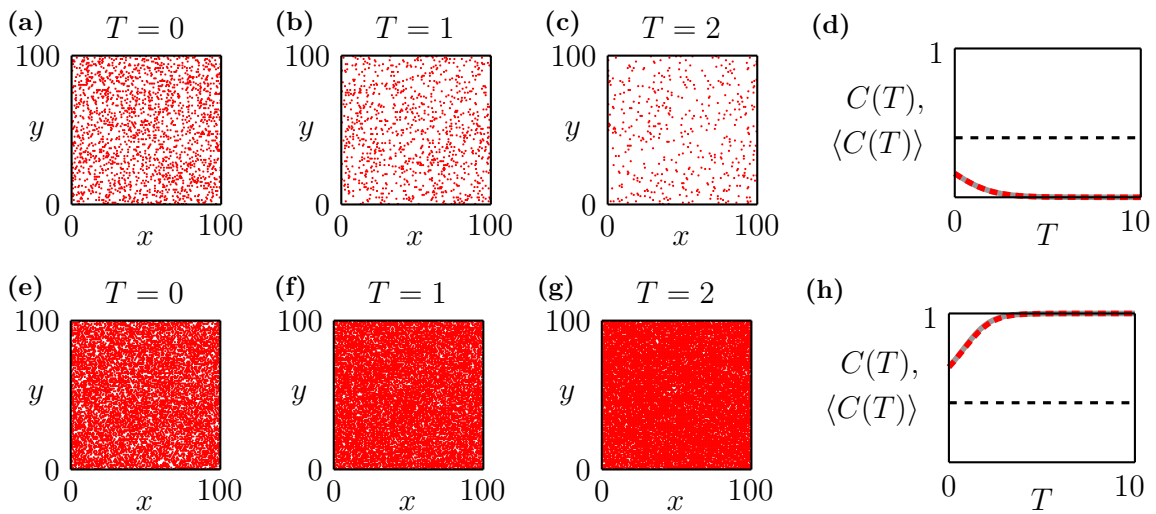


Figure 7: **Comparison of data from the discrete model with the solution of the continuum model for the zero-dimensional initial condition.** (a)–(c) snapshots of discrete simulations at time $T = \lambda t = 0, 1, 2$. At $T = 0$ a fixed number of agents are randomly distributed on the lattice so that $\langle C(0) \rangle = 0.16$. (d) $\langle C(T) \rangle$ (dashed red) and $C(T)$ (solid grey). (e)–(g) snapshots of discrete simulations at time $T = 0, 1, 2$ with $\langle C(0) \rangle = 0.64$. (h) $\langle C(T) \rangle$ (dashed red) and $C(T)$ (solid grey). The dashed black horizontal lines in (d) and (h) are the Allee threshold, $A = 0.4$. Note that we generate 40 identically-prepared realisations to obtain $\langle C(T) \rangle$ in (d) and (h).

We superimpose the solution of Equation (16) with averaged data from the discrete model in Figure 7(d). Again, the continuum model gives a good approximation to the averaged discrete data, and in this case we see that the population becomes extinct.

We now consider the exact same discrete mechanism with a larger initial number of agents giving $\langle C(0) \rangle = 0.64$ in Figure 7(e). Figures 7(f)–(g) again show discrete snapshots as the population evolves, and we observe that $C(T)$ approximates $\langle C(T) \rangle$ well in Figure 7(h). In this case the population survives and grows to reach the maximum density.

Overall, the results in Figures 5–7 confirm that the numerical solution of the continuum model provides a useful way of accurately studying the expected behaviour of the discrete

model. Of interest is that the long-term fate of populations vary with the spatial arrangement of the initial conditions. Our aim now is to study these differences more carefully.

5. Role of dimensionality

Our preliminary results in Section 4 indicate that several factors are at play when we consider the long-term fate of bistable populations. First, the initial number of individuals in the population plays a role. Second, the spatial arrangement of the initial population also plays an important role. Since the initial distribution of the population is given by Equation (11), there are two different ways to vary the initial population size. Either we can adjust the size or shape of the initially-occupied region \mathcal{H} , or we can vary B to alter the initial number of individuals per unit area within \mathcal{H} . In the remainder of this section we investigate all these options systematically.

Results in Figure 8 summarise the long-term outcome of a range of scenarios with the zero-dimensional initial condition. In this case \mathcal{H} corresponds to the entire $L \times L$ domain and $C(0) = B$. We vary the initial condition by systematically varying B , as indicated in Figure 8(a)–(c), and vary the ratio P/M by holding $M = 1$ and varying $P \in [1/1000, 40/1000]$. To systematically study the transition between population extinction to population survival, we take the $(C(0), P/M)$ space and discretize it uniformly into a square mesh, with 51×40 nodes. For each value of $C(0)$ and P/M considered, we generate 40 identically-prepared realisations of the discrete model and we compute the survival probability, $S \in [0, 1]$. That is, we record the fraction of realisations in which the population survives after a sufficiently long period of time \mathcal{T} , which we take to be $\mathcal{T} = \max(30/P, 10^4)$. Figure 8(d) summarises the outcomes of the simulations in terms of a phase diagram. In this case the survival outcome for the continuum model is a simple vertical line at $C(0) = A$. In general we see good agreement between the prediction of survival or extinction between the continuum and discrete models. There is some minor discrepancy as P/M increases. This difference is consistent with the fact that the continuum model P/M has to be sufficiently small otherwise the mean-field approximation is invalid and the solution of the continuum model does not necessarily provide an accurate description of the discrete mechanism (Baker and Simpson 2010; Simpson et al. 2010). In summary, for the zero-dimensional initial condition the long-term population survival depends simply upon whether the initial density is above or below the Allee threshold, as expected.

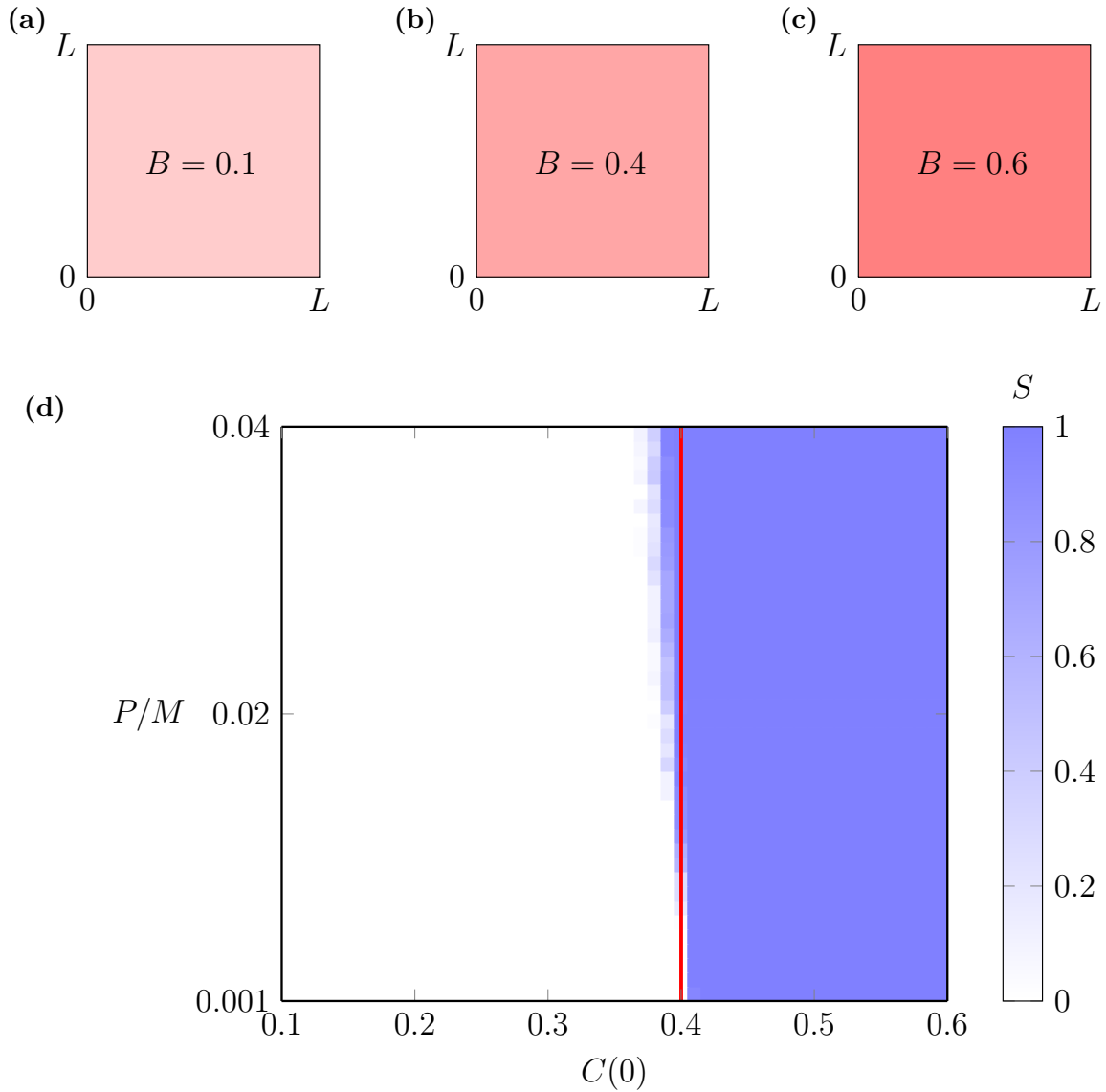


Figure 8: **Phase diagram for extinction/survival with the zero-dimensional initial condition.** (a)–(c) show how we vary the initial density with $C(0) = B$ for this initial condition. (d) Phase diagram of a square mesh with 51×40 nodes for $C(0) \in [1/10, 6/10]$ and $P/M \in [1/1000, 40/1000]$ where $M = 1$. Vertical red line indicates the survival/extinction threshold from the continuum model and the blue shading shows the survival probability S measured by 40 identically-prepared realisations.

When we study long-time extinction or survival using the modelling tools developed in this work, it is useful to note some important differences between the continuum and stochastic approaches. Each numerical solution of the continuum models always leads to the same outcome for the same choice of parameters. In contrast, different identically-prepared realisations of the stochastic model can lead to different outcomes, even when using the same choice of parameters. In practice, this means that the distinction between survival and extinction in the continuum model is straightforward, whereas in the stochastic model we describe the difference between extinction and survival in a probabilistic sense using the concept of survival probability (Surendran et al. 2020; Johnston et al. 2020).

We now explore how the simple outcome for the zero-dimensional initial condition becomes more complicated when we consider different initial spatial arrangements of the population. For the one-dimensional initial condition we first fix $B = 1$ and vary the size of \mathcal{H} by changing the width of the vertical strip, w_1 . Varying the width of the strip leads to a change in the initial density across the entire domain, $C(0) = Bw_1/L$. For example, Figure 9(a)–(c) shows three different one-dimensional initial conditions with $B = 1$ and different widths, w_1 . For these initial conditions we vary the ratio P/M by holding $M = 1$ and varying P . Again, this allows us to consider the $(C(0), P/M)$, which we discretize into a square mesh with 51×40 nodes. Figure 9(b) shows a phase diagram illustrating how the survival probability, S , depends upon $C(0)$ and P/M . The boundary that separates the eventual survival and extinction in the continuum model is shown in solid black, and the survival probability from the discrete simulations is shown in blue shading. Overall, the long-term predictions in terms of survival or extinction are consistent between the continuum and discrete models. For completeness we also show the red vertical line indicating the Allee threshold.

It is interesting to compare the results in Figure 8(d) and Figure 9(d). For the zero-dimensional initial condition long-term survival implies that the initial density is greater than the Allee threshold. In contrast, for the one-dimensional initial condition we observe survival even when $C(0) < A$. Further, in the one-dimensional case we see that the long-term survival is strongly dependent upon P/M whereas in the zero-dimensional case this dependence is less obvious. In Figure 9 we alter $C(0)$ by fixing $B = 1$ and varying w_1 . Another approach is to hold w_1 constant and vary B . Additional results in Appendix D show that these two approaches to varying $C(0)$ lead to very similar outcomes.

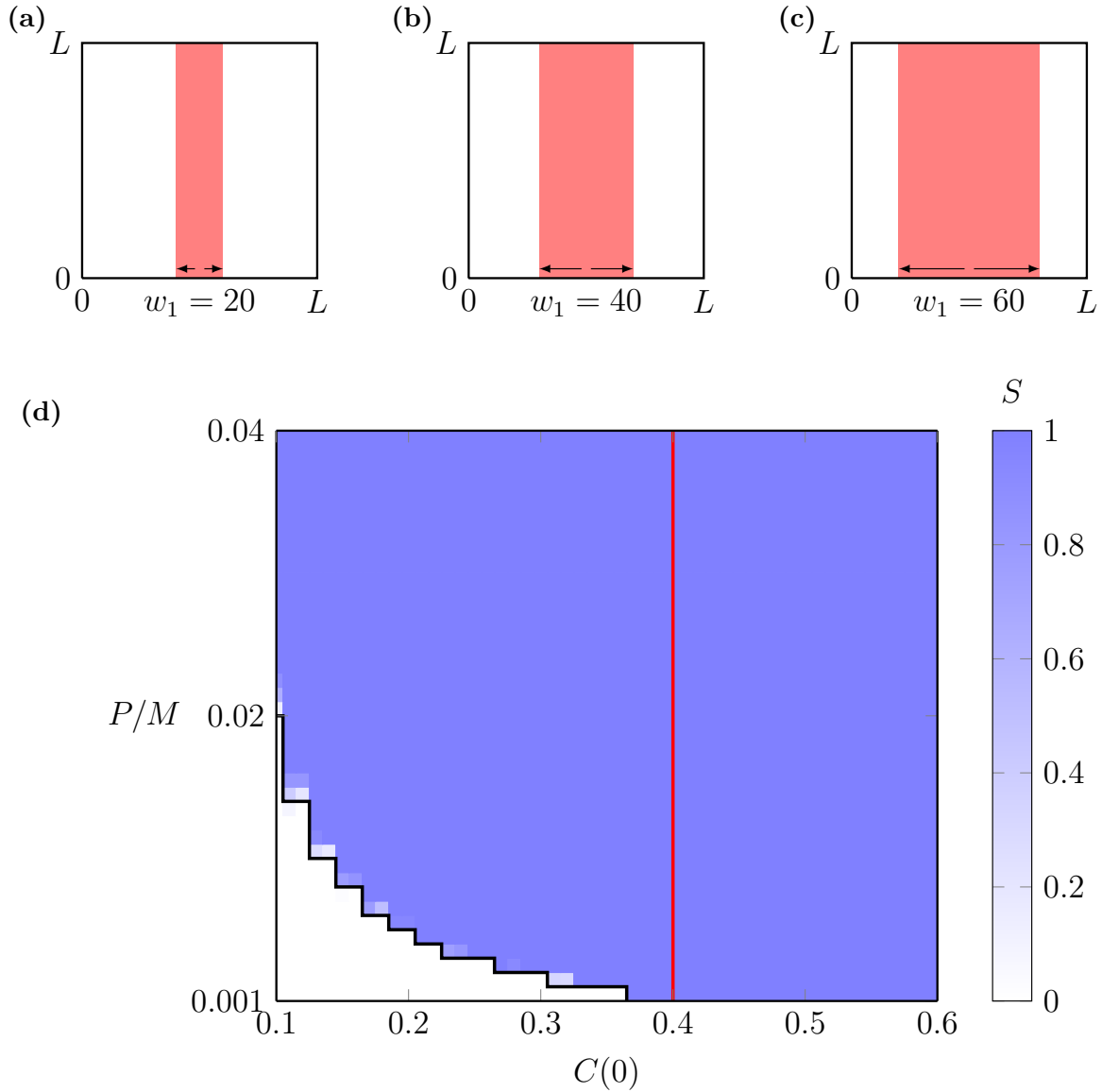


Figure 9: **Phase diagram for extinction/survival with the one-dimensional initial condition.** In (a)–(c) we show three different initial conditions where $C(0) = Bw_1/L$, and we vary w_1 . (d) Phase diagram of a square mesh with 51×40 nodes for $C(0) \in [1/10, 6/10]$ and $P/M \in [1/1000, 40/1000]$ where $M = 1$. Black curve indicates the survival/extinction threshold from the continuum model and the blue shading shows the survival probability S measured by 40 identically-prepared realisations. Vertical red line is $C(0) = 0.4$ which relates to the Allee threshold, $A = 0.4$.

For the two-dimensional initial condition, we fix $B = 1$ and vary the size of \mathcal{H} by changing w where $w = w_1 = w_2$ as shown in Figure 10(a). Varying w allows us to vary the initial density across the entire domain, $C(0) = Bw^2/L^2$. Again, we construct a phase diagram in Figure 10(d) that summarises the long-term survival outcome as a function of $C(0)$ and P/M , by discretizing the $(C(0), P/M)$ space using a square mesh with 51×40 nodes. The phase diagram in Figure 10(d) which is very similar to the phase diagram in Figure 9(d) where we see that the long-term survival depends upon P/M quite strongly, and the distinction between survival and extinction predicted by the continuum limit model is a good approximation of the stochastic simulation data.

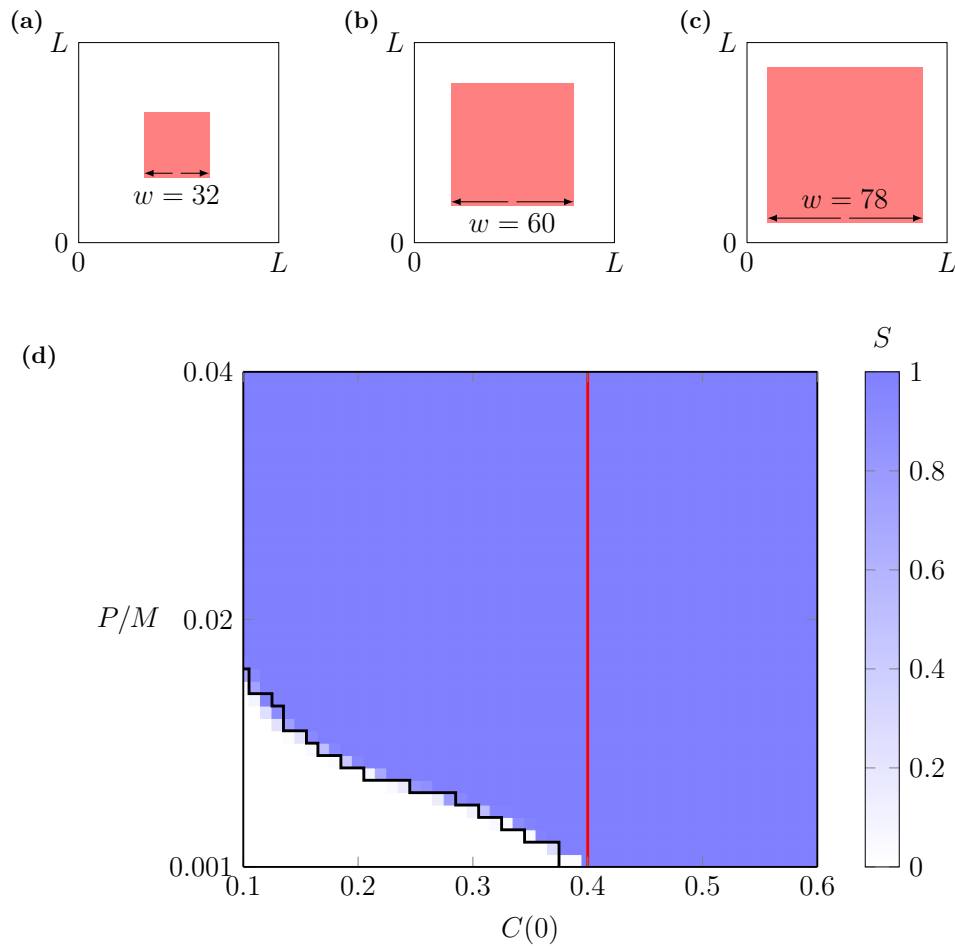


Figure 10: **Phase diagram for extinction/survival with the two-dimensional initial condition.** In (a)–(c) we show three different initial conditions where $C(0) = Bw^2/L^2$, and we vary w . (d) Phase diagram of a square mesh with 51×40 nodes for $C(0) \in [1/10, 6/10]$ and $P/M \in [1/1000, 4/100]$ where $M = 1$. Black curve indicates the survival/extinction threshold from the continuum model and the blue shading shows the survival probability S measured by 40 identically-prepared realisations. Vertical red line is $C(0) = 0.4$ which relates to the Allee threshold, $A = 0.4$.

Results in Figure 8–10 show that the long-term survival of a population depends upon $C(0)$, P/M and the initial arrangement of the population in a complicated manner. To highlight the different fates of various populations, we compare the outcomes from the continuum model from three phase diagrams in Figure 11(a) where we superimpose the boundaries that separate regions of survival and extinction for the zero-dimensional initial condition (red), one-dimensional initial condition (black) and the two-dimensional initial condition (green). Superimposing these curves divides the $(C(0), P/M)$ space into five regions with different long-term outcomes depending on the dimensionality of the initial condition. To emphasise these differences we compare solutions of the continuum model with different values of $C(0)$ and P/M in Figure 11(b)–(g). The six sets of solutions in Figure 11(b)–(g) correspond to various key choices of $C(0)$ and P/M . For example, the profiles in Figure 11(b) relate to region \mathcal{R}_0 where all outcomes lead to extinction regardless of the dimensionality of the initial condition. In contrast, profiles in Figure 11(c) relate to region \mathcal{R}_1 where we see extinction in the zero- and two-dimensional initial conditions, whereas the one-dimensional initial condition leads to survival. This is a very interesting outcome since the discrete mechanism in these three cases is identical, yet the long-term outcome is very different, and depends only upon the dimensionality of the initial condition. Similar differences are highlighted in Figures 11(d)–(g) where we see that differences in long-term survival or extinction of the population often depend on the dimensionality of the initial distribution.

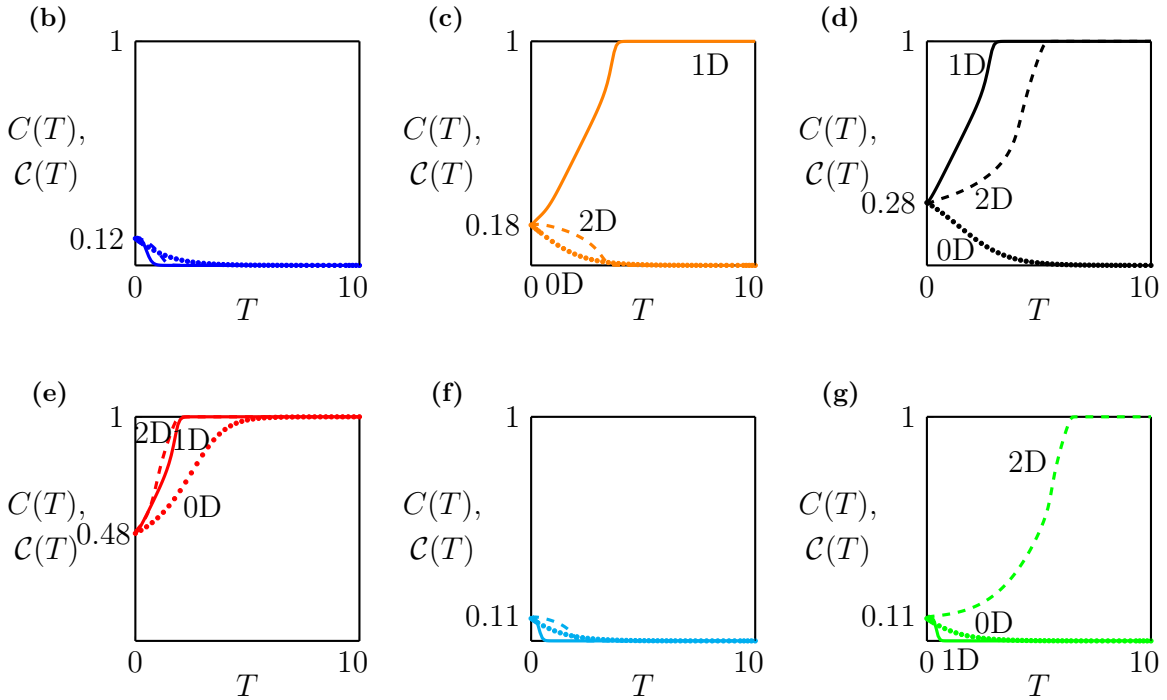
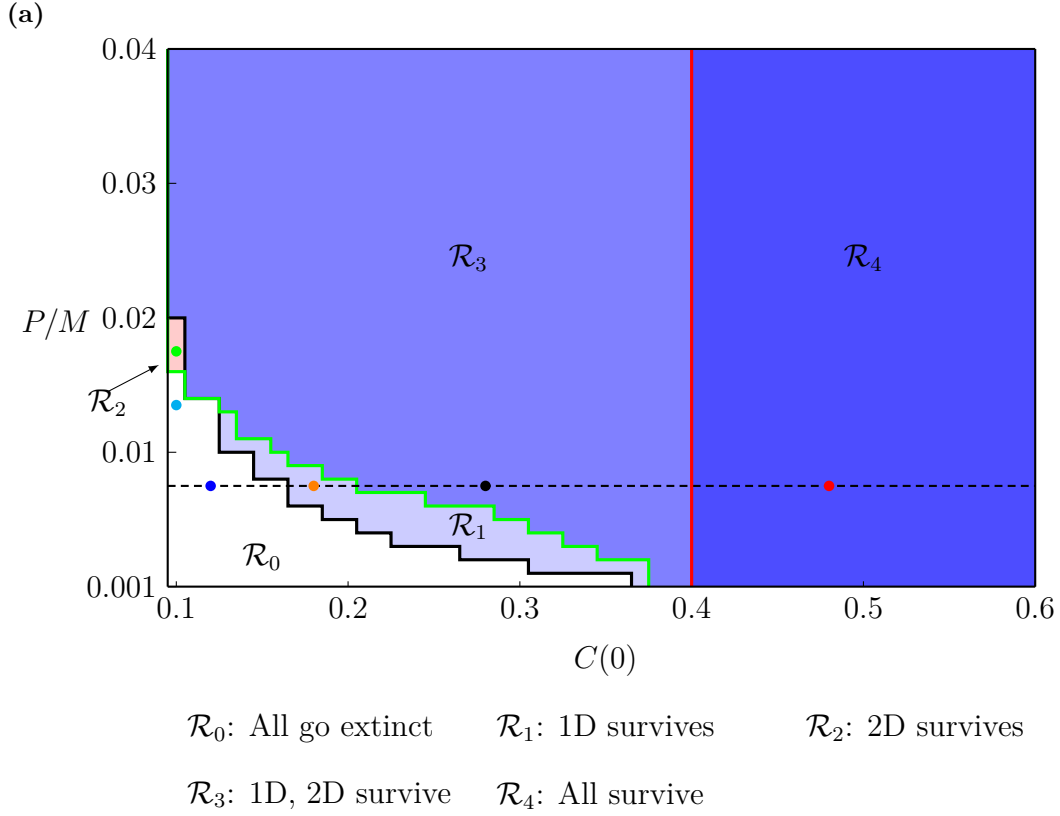


Figure 11: **Role of dimensionality in long-term survival and extinction.** (a) Combined phase diagram where the red, black and green curves highlight the boundaries between extinction and survival for the zero-, one- and two-dimensional initial condition, respectively. Profiles in (b)–(g) show profiles of $C(T)$ and $C(0)$ for six different choices of P/M and $C(0)$. The profile colours in (b)–(g) correspond to the coloured discs superimposed in (a).

6. Conclusions and Outlook

In this work we design, analyse and implement a new two-dimensional stochastic model incorporating movement, birth and death events with crowding effects to study population extinction. The continuum limit of the discrete model is nonlinear RDE which can be used to study a wide range of macroscopic phenomena including linear diffusion, nonlinear diffusion, as well as logistic and bistable growth kinetics. Since the aim of this work is to focus on long term survival or extinction, we choose the movement crowding function to be $G(C) = 1 - C$ which corresponds to macroscopic linear diffusion, and we choose the growth crowding function to be $F(C) = a(1 - C)(C - A)$ which leads to a classical cubic bistable source term with Allee threshold A . Using a range of initial conditions, we show that numerical solutions of the continuum RDE compare well with appropriately averaged data from the discrete model.

The focus of our work is to use the stochastic and continuum models to explore the factors that influence the long-term fate of the bistable population. In particular, we explore three different initial conditions on a finite $L \times L$ domain with periodic boundary conditions. The zero-dimensional initial condition involves distributing agents evenly across the entire $L \times L$ domain, the one-dimensional initial condition involves distributing agents along a vertical strip within the $L \times L$ domain so that the initial density is independent of vertical position in the domain, and the two-dimensional initial condition involves distributing agents within a central square region within the $L \times L$ domain. Our results show that the dimensionality of the population influences the long-term fate of the population in a way that is often overlooked. For example, we show that in many circumstances two populations that are identical with the exception of the dimensionality of their initial condition can lead to very different survival/extinction outcomes.

There are many avenues for extending the work presented in this study. All results presented here focus on a particular choice of domain size L , and the two-dimensional initial conditions are restricted to the case where the initial population is distributed within a square region. Both of these features can be relaxed and similar numerical explorations of the long-term survival or extinction of the populations can be conducted using the software provided on GitHub for both the continuum and discrete models. Another feature of this work that could be explored is the choice of crowding functions. As we pointed out, all simulations here focus on $G(C) = 1 - C$, which gives rise to linear diffusion, and $F(C) = a(1 - C)(C - A)$ which gives rise to the classical cubic bistable term. Other choices of $G(C)$ and $F(C)$ can be incorporated

into the stochastic model to explore how the results presented here depend upon the precise details of these choices of crowding functions. We note that other choices of $G(C)$ lead to different motility mechanisms that are associated with nonlinear diffusion mechanisms, and that these can be important for applications where adhesion (Deroulers et al. 2009) and inertial effects (Zhang et al. 2019) are relevant. While we have not explicitly explored these effects in this work, our framework is sufficiently general that these mechanisms can be incorporated and explore, if required. Another interesting extension would be to consider Allee-type dynamics within more complicated populations that are composed of interacting subpopulations (Simpson et al. 2009). Under these conditions interactions among various subpopulations can also contribute to the eventual survival or extinction of the population (Taylor et al. 2020; Krause and Van Gorder 2020).

Acknowledgements: This work is supported by the Australian Research Council (DP200100177).

Appendix A. Algorithm for discrete simulations

Algorithm 1: Pseudo-code for a single realisation of the stochastic model

```

1 Create a two-dimensional  $I \times J$  hexagonal lattice with some agents where they
  have specific distributions; the total number of lattice site is  $IJ$ ;
2 Set  $t = 0$ ; Calculate total agents  $Q(t)$ ;
3 while  $t < t_{\text{end}}$  and  $Q(t) > 0$  and  $Q(t) \leq IJ$  do
4    $t = t + \tau$ ;
5    $Q(t) = Q(t - \tau)$ ;
6    $B_1 = 0$ ;  $B_2 = 0$ ;
7   Calculate two random variables:  $\beta_1 \sim U[0, 1]$ ,  $\beta_2 \sim U[0, 1]$ ;
8   while  $B_1 < Q(t)$  do
9      $B_1 = B_1 + 1$ ;
10    Randomly choose an agent  $\mathbf{s}$ ;
11    if  $\beta_1 < M$  then
12      Calculate  $\bar{K}_s^{(m)}$  and  $G(\bar{K}_s^{(m)})$ ;
13      Calculate a random variable:  $\gamma_1 \sim U[0, 1]$ ;
14      if  $\gamma_1 < G(\bar{K}_s^{(m)})$  then
15        Randomly choose a vacant site in  $\mathcal{N}_1(\mathbf{s})$  and move agent to chosen
          site
16      else
17        Nothing happens;
18      end
19    else
20      Nothing happens;
21    end
22  end
23  while  $B_2 < N(t)$  do
24     $B_2 = B_2 + 1$ ;
25    Randomly choose an agent  $\mathbf{s}$ ;
26    if  $\beta_2 < P$  then
27      Calculate  $K_s^{(g)}$  and  $F(\bar{K}_s^{(g)})$ ;
28      Calculate a random variable:  $\gamma_2 \sim U[0, 1]$ ;
29      if  $F(\bar{K}_s^{(g)}) > 0$  then
30        if  $\gamma_2 < F(\bar{K}_s^{(g)})$  then
31          Randomly choose a vacant site in  $\mathcal{N}_4(\mathbf{s})$  and place a new agent
            on chosen site;
32           $Q(t) = Q(t) + 1$ 
33        else if  $F(\bar{K}_s^{(g)}) < 0$  then
34          if  $\gamma_2 < -F(\bar{K}_s^{(g)})$  then
35            Remove agent;
36             $Q(t) = Q(t) - 1$ ;
37          else
38            Nothing happens;
39          end
40        else
41          Nothing happens;
42        end
43      end
44  end

```

Appendix B. Derivation of the continuum limit

The expected change in occupancy of site \mathbf{s} during the time interval from t to $t + \tau$ is

$$\begin{aligned} \delta(\overline{C}_{\mathbf{s}}) &= \frac{M}{|\mathcal{N}_1|} (1 - \overline{C}_{\mathbf{s}}) \sum_{s' \in \mathcal{N}_1\{\mathbf{s}\}} C_{s'} \frac{G(\overline{K}_{s'}^{(m)})}{1 - \overline{K}_{s'}^{(m)}} - M \overline{C}_{\mathbf{s}} G(\overline{K}_{\mathbf{s}}^{(m)}) \\ &\quad + \frac{P}{|\mathcal{N}_4|} (1 - \overline{C}_{\mathbf{s}}) \sum_{s' \in \mathcal{N}_4\{\mathbf{s}\}} \mathbb{H}(F(\overline{K}_{s'}^{(g)})) C_{s'} \frac{F(\overline{K}_{s'}^{(g)})}{1 - \overline{K}_{s'}^{(g)}} - (1 - \mathbb{H}(F(\overline{K}_{\mathbf{s}}^{(g)}))) P \overline{C}_{\mathbf{s}} F(\overline{K}_{\mathbf{s}}^{(g)}). \end{aligned} \quad (\text{B.1})$$

For convenience, we omit the overlines on notations in the following content. As we know that the continuum limit of the last two terms in Equation (B.1) leads to a source term $\lambda C F(C)$ (Jin et al. 2016), we focus on the movement mechanism, that is, the first two terms on the right hand side of Equation (B.1).

The site \mathbf{s} located at (x, y) has six nearest neighbouring sites: site \mathbf{s}_1 with $(x - \Delta, y)$; site \mathbf{s}_2 with $(x + \Delta, y)$; site \mathbf{s}_3 with $(x - \Delta/2, y + \Delta\sqrt{3}/2)$; site \mathbf{s}_4 with $(x + \Delta/2, y + \Delta\sqrt{3}/2)$; site \mathbf{s}_5 with $(x - \Delta/2, y - \Delta\sqrt{3}/2)$ and site \mathbf{s}_6 with $(x + \Delta/2, y - \Delta\sqrt{3}/2)$. That is, $\mathcal{N}_1 = \{\mathbf{s}_1, \mathbf{s}_2, \mathbf{s}_3, \mathbf{s}_4, \mathbf{s}_5, \mathbf{s}_6\}$.

Expanding the occupancy of these sites in a truncated Taylor series gives

$$C_{\mathbf{s}_1} = C_{\mathbf{s}} - \frac{\partial C_{\mathbf{s}}}{\partial x} \Delta + \frac{\partial^2 C_{\mathbf{s}}}{\partial x^2} \frac{\Delta^2}{2} + \mathcal{O}(\Delta^3), \quad (\text{B.2})$$

$$C_{\mathbf{s}_2} = C_{\mathbf{s}} + \frac{\partial C_{\mathbf{s}}}{\partial x} \Delta + \frac{\partial^2 C_{\mathbf{s}}}{\partial x^2} \frac{\Delta^2}{2} + \mathcal{O}(\Delta^3), \quad (\text{B.3})$$

$$C_{\mathbf{s}_3} = C_{\mathbf{s}} - \frac{\partial C_{\mathbf{s}}}{\partial x} \frac{\Delta}{2} + \frac{\partial C_{\mathbf{s}}}{\partial y} \frac{\sqrt{3}\Delta}{2} + \left[\frac{1}{4} \frac{\partial^2 C_{\mathbf{s}}}{\partial x^2} + \frac{3}{4} \frac{\partial^2 C_{\mathbf{s}}}{\partial y^2} - \frac{\sqrt{3}}{2} \frac{\partial^2 C_{\mathbf{s}}}{\partial x \partial y} \right] \frac{\Delta^2}{2} + \mathcal{O}(\Delta^3), \quad (\text{B.4})$$

$$C_{\mathbf{s}_4} = C_{\mathbf{s}} + \frac{\partial C_{\mathbf{s}}}{\partial x} \frac{\Delta}{2} + \frac{\partial C_{\mathbf{s}}}{\partial y} \frac{\sqrt{3}\Delta}{2} + \left[\frac{1}{4} \frac{\partial^2 C_{\mathbf{s}}}{\partial x^2} + \frac{3}{4} \frac{\partial^2 C_{\mathbf{s}}}{\partial y^2} + \frac{\sqrt{3}}{2} \frac{\partial^2 C_{\mathbf{s}}}{\partial x \partial y} \right] \frac{\Delta^2}{2} + \mathcal{O}(\Delta^3), \quad (\text{B.5})$$

$$C_{\mathbf{s}_5} = C_{\mathbf{s}} - \frac{\partial C_{\mathbf{s}}}{\partial x} \frac{\Delta}{2} - \frac{\partial C_{\mathbf{s}}}{\partial y} \frac{\sqrt{3}\Delta}{2} + \left[\frac{1}{4} \frac{\partial^2 C_{\mathbf{s}}}{\partial x^2} + \frac{3}{4} \frac{\partial^2 C_{\mathbf{s}}}{\partial y^2} + \frac{\sqrt{3}}{2} \frac{\partial^2 C_{\mathbf{s}}}{\partial x \partial y} \right] \frac{\Delta^2}{2} + \mathcal{O}(\Delta^3), \quad (\text{B.6})$$

$$C_{\mathbf{s}_6} = C_{\mathbf{s}} + \frac{\partial C_{\mathbf{s}}}{\partial x} \frac{\Delta}{2} - \frac{\partial C_{\mathbf{s}}}{\partial y} \frac{\sqrt{3}\Delta}{2} + \left[\frac{1}{4} \frac{\partial^2 C_{\mathbf{s}}}{\partial x^2} + \frac{3}{4} \frac{\partial^2 C_{\mathbf{s}}}{\partial y^2} - \frac{\sqrt{3}}{2} \frac{\partial^2 C_{\mathbf{s}}}{\partial x \partial y} \right] \frac{\Delta^2}{2} + \mathcal{O}(\Delta^3). \quad (\text{B.7})$$

Thus, the averaged occupancy of site \mathbf{s}_1 is

$$\begin{aligned} K_{\mathbf{s}_1}^{(m)} &= \frac{1}{6} \sum_{s'' \in \mathcal{N}_1\{\mathbf{s}'\}} C_{s''} \\ &= C_{\mathbf{s}_1} + \left(\frac{\partial^2 C_{\mathbf{s}_1}}{\partial x^2} + \frac{\partial^2 C_{\mathbf{s}_1}}{\partial y^2} \right) \frac{\Delta^2}{4} + \mathcal{O}(\Delta^3), \\ &= C_{\mathbf{s}} - \frac{\partial C_{\mathbf{s}}}{\partial x} \Delta + \frac{\partial^2 C_{\mathbf{s}}}{\partial x^2} \frac{\Delta^2}{2} + \left(\frac{\partial^2 C_{\mathbf{s}}}{\partial x^2} + \frac{\partial^2 C_{\mathbf{s}}}{\partial y^2} \right) \frac{\Delta^2}{4} + \mathcal{O}(\Delta^3). \end{aligned} \quad (\text{B.8})$$

For simplification we will use two notations

$$\mathcal{A} = \left(\frac{\partial^2 C_{\mathbf{s}}}{\partial x^2} + \frac{\partial^2 C_{\mathbf{s}}}{\partial y^2} \right) \frac{\Delta^2}{4}, \quad \mathcal{B} = \left(\left(\frac{\partial C_{\mathbf{s}}}{\partial x} \right)^2 + \left(\frac{\partial C_{\mathbf{s}}}{\partial y} \right)^2 \right) \frac{\Delta^2}{4}, \quad (\text{B.9})$$

and rewrite Equation (B.8) as $K_{\mathbf{s}_1}^{(m)} = C_{\mathbf{s}} + \tilde{C}_{\mathbf{s}_1}$, where $\tilde{C}_{\mathbf{s}_1} \sim \mathcal{O}(\Delta)$. Subsequently, the movement crowding function at \mathbf{s}_1 can be expanded as

$$\begin{aligned} G(K_{\mathbf{s}_1}^{(m)}) &= G(C_{\mathbf{s}} + \tilde{C}_{\mathbf{s}_1}), \\ &= G(C_{\mathbf{s}}) + \frac{dG(C_{\mathbf{s}})}{dC} \tilde{C}_{\mathbf{s}_1} + \frac{d^2G(C_{\mathbf{s}})}{dC^2} \frac{\tilde{C}_{\mathbf{s}_1}^2}{2}. \end{aligned} \quad (\text{B.10})$$

The expansions of $G(K_{\mathbf{s}_2}^{(m)})$, $G(K_{\mathbf{s}_3}^{(m)})$, ..., $G(K_{\mathbf{s}_6}^{(m)})$ have similar forms to (B.10). We then go back to the first term on the right hand side of (B.1), which gives

$$\frac{M}{6} (1 - C_{\mathbf{s}}) \sum_{s' \in \mathcal{N}_1\{\mathbf{s}\}} C_{s'} \frac{G(K_{s'}^{(m)})}{1 - K_{s'}^{(m)}}. \quad (\text{B.11})$$

For convenience we further drop the \mathbf{s} notation so that $C_{\mathbf{s}}$ becomes C and $C_{\mathbf{s}_1}$ becomes C_1 . Subsequently, (B.11) becomes

$$\frac{M}{6} (1 - C) \sum_{i=1}^6 C_i \frac{G(K_{\mathbf{s}_i}^{(m)})}{1 - K_{\mathbf{s}_i}^{(m)}}. \quad (\text{B.12})$$

Expanding the term related to site \mathbf{s}_1 in (B.12) gives

$$\begin{aligned} & \frac{M}{6} (1 - C) (C + \tilde{C}_1 - \mathcal{A}) \frac{\left(G(C) + G'(C) \tilde{C}_1 + G''(C) \frac{\tilde{C}_1^2}{2} \right)}{1 - (C + \tilde{C}_1)} \\ &= \frac{M}{6} (1 - C) (C + \tilde{C}_1 - \mathcal{A}) \left(G(C) + G'(C) \tilde{C}_1 + G''(C) \frac{\tilde{C}_1^2}{2} \right) \left(\frac{1}{1 - C} + \frac{\tilde{C}_1}{(1 - C)^2} + \frac{\tilde{C}_1^2}{(1 - C)^3} \right) + \mathcal{O}(\Delta^3) \\ &= \frac{M}{6} (C + \tilde{C}_1 - \mathcal{A}) \left(G(C) + G'(C) \tilde{C}_1 + G''(C) \frac{\tilde{C}_1^2}{2} \right) \left(1 + \frac{\tilde{C}_1}{1 - C} + \frac{\tilde{C}_1^2}{(1 - C)^2} \right) + \mathcal{O}(\Delta^3) \\ &= \frac{M}{6} \left[CG(C) + \left(CG'(C) + \frac{G(C)}{1 - C} \right) \tilde{C}_1 + \left(\frac{G(C)}{(1 - C)^2} + \frac{G'(C)}{1 - C} + \frac{CG''(C)}{2} \right) \tilde{C}_1^2 - G(C) \mathcal{A} \right] + \mathcal{O}(\Delta^3). \end{aligned}$$

The terms related to other sites can be obtained in a similar way. Therefore, expanding all

terms in (B.12) and neglecting terms of order $\mathcal{O}(\Delta^3)$ gives

$$\frac{M}{6} \left[6CG(C) + \left(CG'(C) + \frac{G(C)}{1-C} \right) \sum_{k=1}^6 \tilde{C}_k + \left(\frac{G(C)}{(1-C)^2} + \frac{G'(C)}{1-C} + \frac{CG''(C)}{2} \right) \sum_{k=1}^6 \tilde{C}_k^2 - 6G(C)\mathcal{A} \right]. \quad (\text{B.13})$$

Furthermore, since we have

$$\begin{aligned} \sum_{k=1}^6 \tilde{C}_k &= 12 \left(\frac{\partial^2 C}{\partial x^2} + \frac{\partial^2 C}{\partial y^2} \right) \frac{\Delta^2}{4} + \mathcal{O}(\Delta^3), \\ &= 12\mathcal{A} + \mathcal{O}(\Delta^3), \end{aligned} \quad (\text{B.14})$$

and

$$\begin{aligned} \sum_{k=1}^6 \tilde{C}_k^2 &= 12 \left(\left(\frac{\partial C}{\partial x} \right)^2 + \left(\frac{\partial C}{\partial y} \right)^2 \right) \frac{\Delta^2}{4} + \mathcal{O}(\Delta^3), \\ &= 12\mathcal{B} + \mathcal{O}(\Delta^3), \end{aligned} \quad (\text{B.15})$$

Equation (B.13) becomes

$$MCG(C) + M \left(2CG'(C) - G(C) + \frac{2G(C)}{1-C} \right) \mathcal{A} + M \left(CG''(C) + \frac{2G(C)}{(1-C)^2} + \frac{2G'(C)}{1-C} \right) \mathcal{B} + \mathcal{O}(\Delta^3). \quad (\text{B.16})$$

Remind that the second term in (B.1) is

$$\begin{aligned} MCG(\bar{K}_s^{(m)}) &= MCG(C) + MCG'(C)\tilde{C}, \\ &= MCG(C) + MCG'(C)\mathcal{A} + \mathcal{O}(\Delta^3). \end{aligned} \quad (\text{B.17})$$

Then combining (B.16) and (B.17) gives

$$\begin{aligned} \delta(C_s) &= \left(CG'(C) - G(C) + \frac{2G(C)}{1-C} \right) M\mathcal{A} + \left(CG''(C) + \frac{2G(C)}{(1-C)^2} + \frac{2G'(C)}{1-C} \right) M\mathcal{B} + \mathcal{O}(\Delta^3), \\ &= \left(CG'(C) + \frac{1+C}{1-C}G(C) \right) M\mathcal{A} + \left(CG''(C) + \frac{2G(C)}{(1-C)^2} + \frac{2G'(C)}{1-C} \right) M\mathcal{B} + \mathcal{O}(\Delta^3). \end{aligned} \quad (\text{B.18})$$

Dividing both sides of the resulting expression by τ , and letting $\Delta \rightarrow 0$ and $\tau \rightarrow 0$ jointly, with the ratio Δ^2/τ held constant, leads to the following nonlinear reaction-diffusion equation,

$$\frac{\partial C}{\partial t} = D_0 \nabla \cdot \left[\left(CG'(C) + \frac{1+C}{1-C}G(C) \right) \nabla C \right] + \lambda CF(C), \quad (\text{B.19})$$

where

$$D_0 = \frac{M}{4} \lim_{\Delta, \tau \rightarrow 0} \frac{\Delta^2}{\tau}, \quad \lambda = \lim_{\tau \rightarrow 0} \frac{P}{\tau}. \quad (\text{B.20})$$

If we define

$$D(C) = CG'(C) + \frac{1+C}{1-C}G(C), \quad (\text{B.21})$$

then the continuum limit is written as

$$\frac{\partial C}{\partial t} = D_0 \nabla \cdot [D(C) \nabla C] + \lambda CF(C). \quad (\text{B.22})$$

Appendix C. Numerical methods

Here, we introduce the method of lines to numerically calculate solutions of the PDE

$$\frac{\partial C}{\partial t} = D_0 \nabla^2 C + R(C), \quad (\text{C.1})$$

on a square domain $\Omega = \{(x, y), 0 < x < L, 0 < y < L\}$. We first discretise the spatial derivative in Equation (C.1) with an $(I + 1) \times (I + 1)$ mesh. Nodes on the mesh are uniformly distributed with spacing $\delta x > 0$ and indexed by x_i and y_j with $i = 0, 1, 2, \dots, I$ and $j = 0, 1, 2, \dots, I$ satisfying $I = L/\delta x$. Then we leave the time derivative continuous and obtain

$$\frac{dC_{i,j}}{dt} = \frac{D_0}{\delta x^2} (C_{i+1,j} + C_{i-1,j} + C_{i,j+1} + C_{i,j-1} - 4C_{i,j}) + R(C_{i,j}). \quad (\text{C.2})$$

This equation is valid for interior nodes, and is modified on the boundary nodes to simulate periodic boundary conditions. This system of $I \times I$ coupled ordinary differential equations is then integrated through time using MATLABs function `ode45` (MATLAB 2020). Following similar steps, we can also calculate the numerical solution of the PDE

$$\frac{\partial C}{\partial t} = D_0 \frac{\partial^2 C}{\partial x^2} + R(C). \quad (\text{C.3})$$

Appendix D. Phase diagrams with $B \neq 1$

Instead of varying the size of \mathcal{H} , we now vary $C(0)$ by varying B . We constrain the region \mathcal{H} as a vertical strip with width $w_1 = 64$, as shown in Figure S1(a). As $C(0) = Bw_1/L$ where we fix $w_1/L = 0.64$, the initial density $C(0)$ varies from 0.192 to 0.64 when B varies from 0.3 to 1 as illustrated in Figure S1(a)–(c). We further vary P/M by holding $M = 1$ and varying $P \in [1/1000, 4/100]$ so that $(C(0), P)$ space is discretised into a square mesh with 36×40 nodes. Figure S1(d) shows a phase diagram illustrating how the survival probability, S , depends upon $C(0)$ and P/M . The boundary that separates the eventual survival and extinction in the continuum model is shown in solid black, and the survival probability from the discrete simulations is shown in blue shading. Again, the long-term predictions in terms of survival or extinction are consistent between the continuum and discrete models. The red solid line is $C(0) = 0.4$ and the red dashed line is $B = 0.4$. They both indicate the Allee threshold $A = 0.4$, where the solid line $C(0) = 0.4$ indicates a threshold of survival in the sense of global density and the dashed line $B = 0.4$ indicates a threshold of survival in the sense of local density.

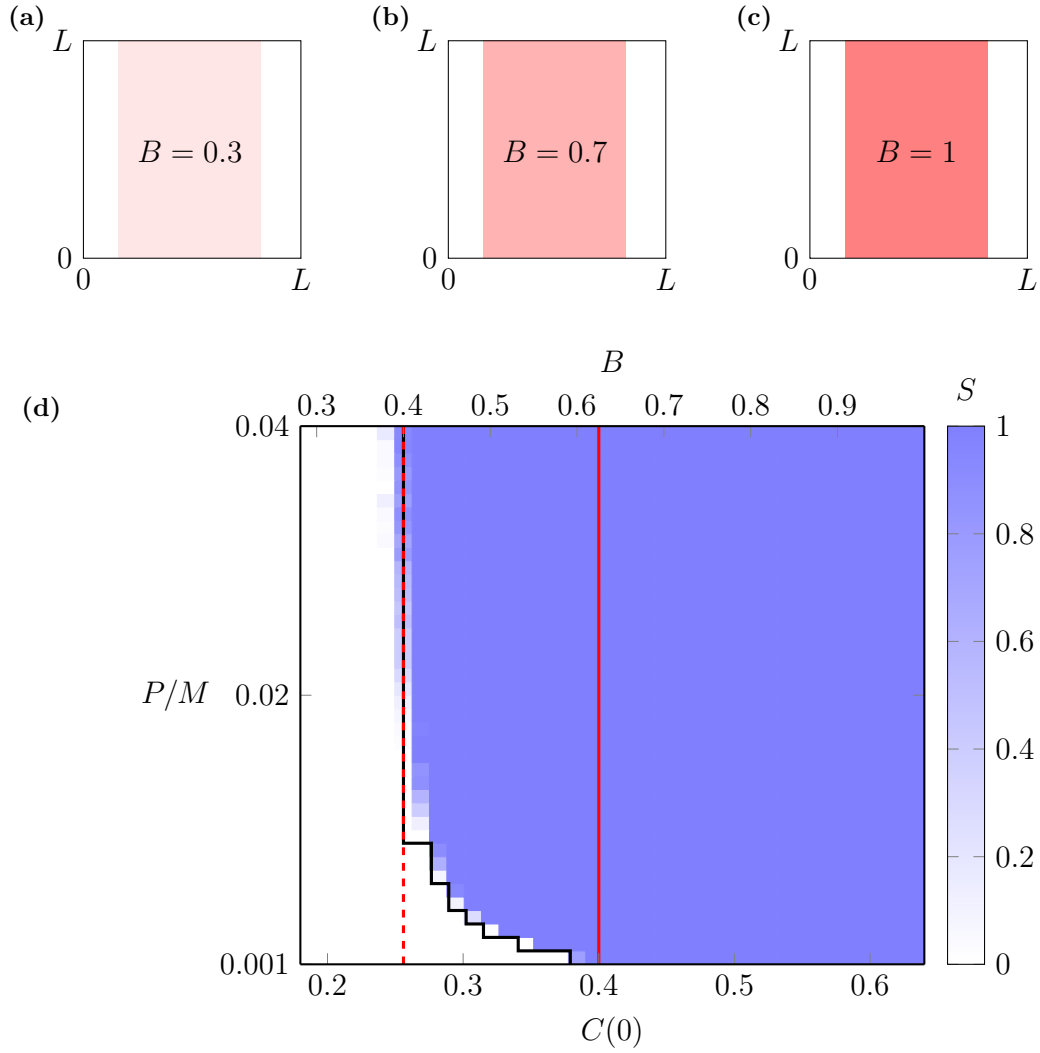


Figure S1: **Phase diagram for extinction/survival with the one-dimensional initial condition.** In (a)–(c) we show three different initial conditions where $C(0) = Bw_1/L$, and we fix $w_1 = 64$ and vary B . (d) Phase diagram on a square mesh with 36×40 nodes for $C(0) \in [0.192, 0.64]$ and $P/M \in [1/1000, 4/100]$. Black curve indicates the survival/extinction threshold from the continuum model and the blue shading shows the survival probability S measured by 40 identically-prepared realisations. Vertical solid red line is $C(0) = 0.4$. Vertical dashed line is $B = 0.4$. They both relate to the Allee threshold, $A = 0.4$.

Next, we constrain the region \mathcal{H} as a square region with width $w = w_1 = w_2 = 80$ in Figure S2(a)–(c). As $C(0) = Bw^2/L^2$ where we fix $w^2/L^2 = 0.64$, the initial density $C(0)$ again varies from 0.192 to 0.64 when B varies from 0.3 to 1. We again change P/M by holding $M = 1$ and varying $P \in [1/1000, 4/100]$ so that $(C(0), P/M)$ space is discretised into a square mesh with 36×40 nodes. With this initial condition we again construct a phase diagram summarising the long-term survival outcome as a function of $C(0)$ and P/M in Figure S2(d), which is very similar to the phase diagram in Figure S1(d) where we see that the long-term survival depends on P/M and the two red lines indicating the Allee threshold.

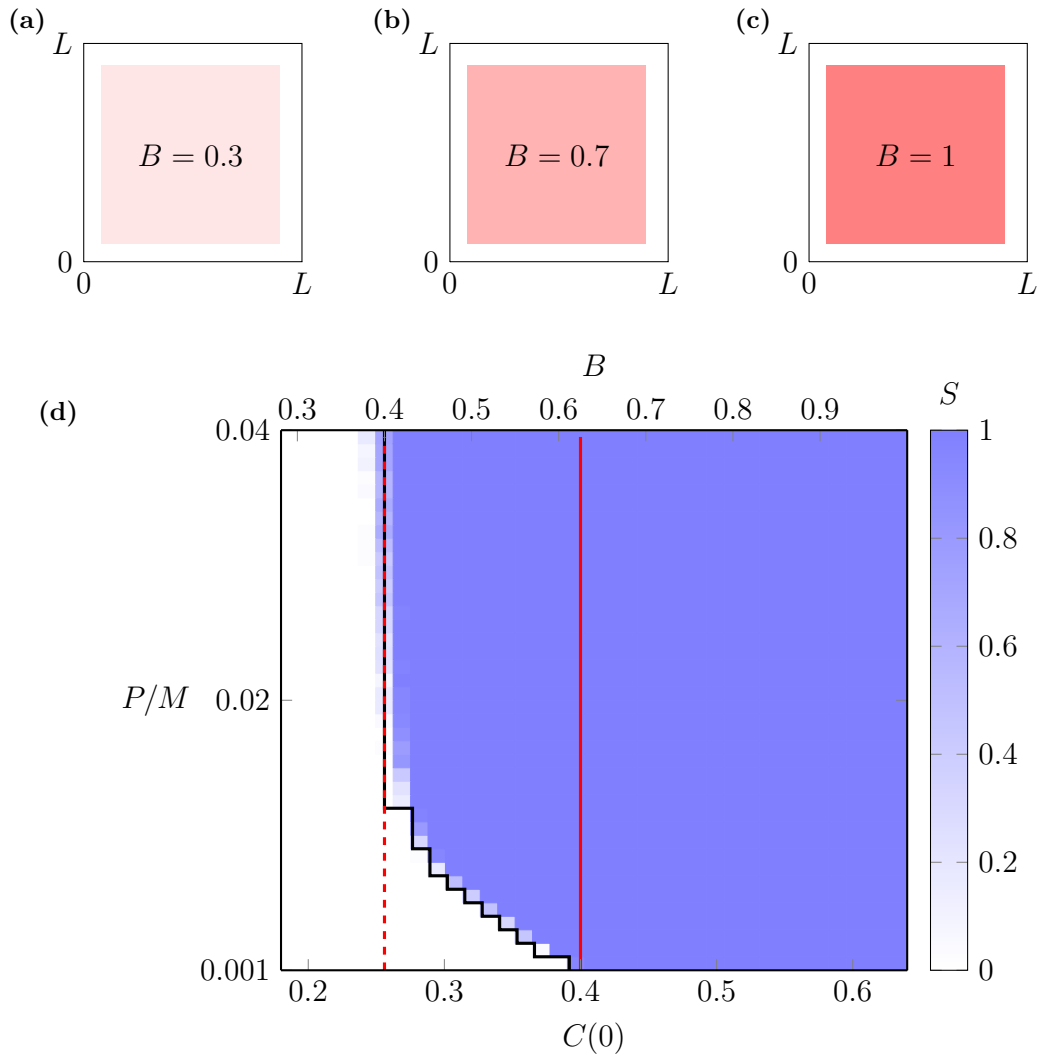


Figure S2: **Phase diagram for extinction/survival with the one-dimensional initial condition.** In (a)–(c) we show three different initial conditions where $C(0) = Bw^2/L^2$, and we fix $w = 80$ and vary B . (d) Phase diagram on a square mesh with 36×40 nodes for $C(0) \in [0.192, 0.64]$ and $P/M \in [1/1000, 4/100]$. Black curve indicates the survival/extinction threshold from the continuum model and the blue shading shows the survival probability S measured by 40 identically-prepared realisations. Vertical solid red line is $C(0) = 0.4$. Vertical dashed line is $B = 0.4$. They both relate to the Allee threshold, $A = 0.4$.

To highlight the different fates of various populations, we compare the outcomes from the continuum model from three phase diagrams in Figure S3(a), where we superimpose the boundaries that separate regions of survival and extinction for the zero-dimensional initial condition (red), one-dimensional initial condition (black) and the two-dimensional initial condition (green). Superimposing these curves divides the $(C(0), P/M)$ plane into four regions with different long-term outcomes depending on the dimensionality of the initial conditions. To emphasise these differences we compare solutions of the continuum model with different values of $C(0)$ and P/M in S3(b)–(g). The six sets of solutions in Figure S3(b)–(g) correspond to various illustrative choices of $C(0)$ and P/M . For example, the profiles in Figure S3(b) related to region \mathcal{R}_0 all lead to extinction regardless of the dimensionality of the initial condition, whereas the profiles in Figure S3(c) related to region \mathcal{R}_1 lead to extinction for the zero- and two-dimensional conditions, whereas the one-dimensional initial condition leads to survival.

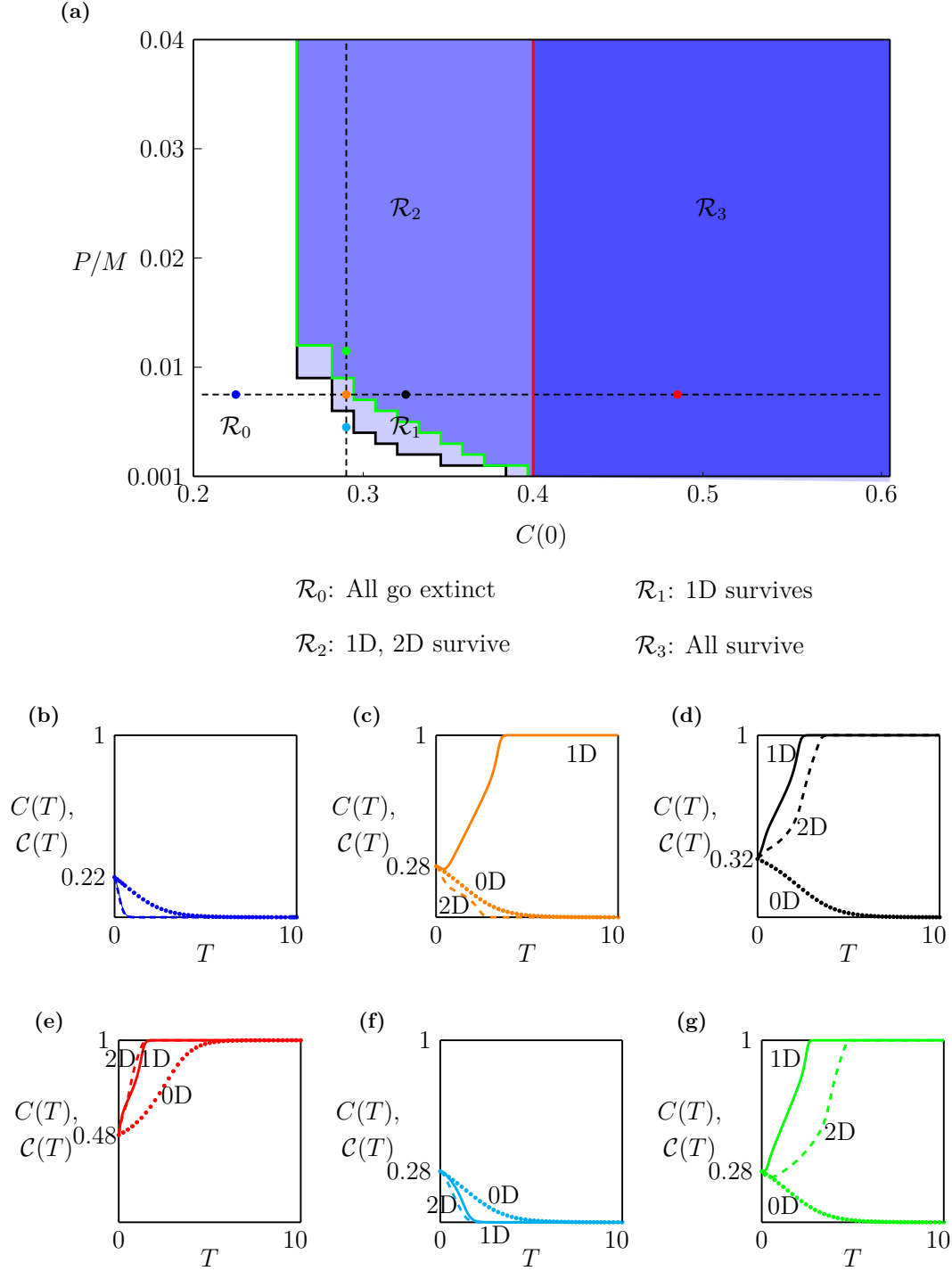


Figure S3: **Role of dimensionality in long-term survival and extinction.** (a) Combined phase diagram where the red, black and green curves highlight the boundaries between extinction and survival for the zero-, one- and two-dimensional initial condition, respectively. Profiles in (b)–(g) show profiles of $C(T)$ and $\mathcal{C}(T)$ for six different choices of P/M and $C(0)$. The profile colours in (b)–(g) correspond to the coloured discs superimposed in (a).

References

- Allee, W.C., Bowen, E.S., 1932. Studies in animal aggregations: Mass protection against colloidal silver among goldfishes. *Journal of Experimental Zoology*. 61, 185–207.
- Arroyo-Esquivel, J., Hastings, A., 2020. Spatial dynamics and spread of ecosystem engineers: Two patch analysis. *Bulletin of Mathematical Biology*. 82, 149.
- Baker, R.E., Simpson, M.J., 2010. Correcting mean-field approximations for birth-death-movement processes. *Physical Review E*. 82, 041905.
- Böttger, K., Hatzikirou, H., Voss-Böhme, A., Cavalcanti-Adam, E.A., Herrero, M.A., Deutsch, A., 2015. An emerging Allee effect is critical for tumor initiation and persistence. *PLoS Computational Biology*. 11, e1004366.
- Chaplain, M.A.J., Lorenzi, T., Macfarlane, F.R., 2020. Bridging the gap between individual-based and continuum models of growing cell populations. *Journal of Mathematical Biology*. 80, 343–371.
- Courchamp, F., Berec, L., Gascoigne, J., 2008. *Allee effects in ecology and conservation*. Oxford University Press, Oxford.
- Courchamp, F., Clutton-Brock, T., Grenfell, B., 1999. Inverse density dependence and the Allee effect. *Trends in Ecology & Evolution*. 14, 405–410.
- Deroulers, C., Aubert, M., Badoual, M., Grammaticos, B., 2009. Modeling tumor cell migration: From microscopic to macroscopic models. *Physical Review E*. 79, 031917.
- Drake, J.M., 2004. Allee effects and the risk of biological invasion. *Risk Analysis*. 24, 795–802.
- Edelstein-Keshet, L., 2005. *Mathematical models in biology*. SIAM, Philadelphia.
- Fadai, N.T., Johnston, S.T., Simpson, M.J., 2020. Unpacking the Allee effect: determining individual-level mechanisms that drive global population dynamics. *Proceedings of the Royal Society A: Mathematical, Physical and Engineering Sciences*. 476, 20200350.
- Fadai, N.T., Simpson, M.J., 2020. Population dynamics with threshold effects give rise to a diverse family of Allee effects. *Bulletin of Mathematical Biology*. 82, 74.

- Fife, P.C., 1979. Long time behavior of solutions of bistable nonlinear diffusion equations. *Archive for Rational Mechanics and Analysis*. 70, 31–36.
- Fisher, R.A., 1937. The wave of advance of advantageous genes. *Annals of Eugenics*. 7, 355–369.
- Hastings, A., Cuddington, K., Davies, K.F., Dugaw, C.J., Elmendorf, S., Freestone, A., Harrison, S., Holland, M., Lambrinos, J., Malvadkar, U., Melbourne, B.A., Moore, K., Taylor, C., Thomson, D., 2005. The spatial spread of invasions: new developments in theory and evidence. *Ecology Letters*. 8, 91–101.
- Hughes, B.D., 1995. Random walks and random environments: random walks. volume 1. Oxford University Press, Oxford.
- Jin, W., Penington, C.J., McCue, S.W., Simpson, M.J., 2016. Stochastic simulation tools and continuum models for describing two-dimensional collective cell spreading with universal growth functions. *Physical Biology*. 13, 056003.
- Johnston, S.T., Baker, R.E., McElwain, D.L.S., Simpson, M.J., 2017. Co-operation, competition and crowding: A discrete framework linking Allee kinetics, nonlinear diffusion, shocks and sharp-fronted travelling waves. *Scientific Reports*. 7, 42134.
- Johnston, S.T., Simpson, M.J., Crampin, E.J., 2020. Predicting population extinction in lattice-based birth-death-movement models. *Proceedings of the Royal Society A: Mathematical, Physical and Engineering Sciences*. 476, 20200089.
- Kot, M., 2001. *Elements of mathematical ecology*. Cambridge University Press, Cambridge.
- Krause, A.L., Van Gorder, R.A., 2020. A non-local cross-diffusion model of population dynamics II: Exact, approximate, and numerical traveling waves in single- and multi-species populations. *Bulletin of Mathematical Biology*. 82, 113.
- Lewis, M.A., Kareiva, P., 1993. Allee dynamics and the spread of invading organisms. *Theoretical Population Biology*. 43, 141–158.
- Macfarlane, F.R., Lorenzi, T., Chaplain, M.A.J., 2018. Modelling the immune response to cancer: An individual-based approach accounting for the difference in movement between inactive and activated T cells. *Bulletin of Mathematical Biology*. 80, 1539–1562.

- Maini, P.K., McElwain, D.L.S., Leavesley, D., 2004a. Traveling wave model to interpret a wound-healing cell migration assay for human peritoneal mesothelial cells. *Tissue Engineering*. 10, 475–482.
- Maini, P.K., McElwain, D.L.S., Leavesley, D., 2004b. Travelling waves in a wound healing assay. *Applied Mathematics Letters*. 17, 575–580.
- MATLAB, 2020. ode45 documentation. URL: <https://www.mathworks.com/help/matlab/ref/ode45.html>.
- Murray, J.D., 2002. *Mathematical biology: I. An introduction*. Springer, New York.
- Neufeld, Z., von Witt, W., Lakatos, D., Wang, J., Hegedus, B., Czirok, A., 2017. The role of Allee effect in modelling post resection recurrence of glioblastoma. *PLoS Computational Biology*. 13, e1005818.
- Perumpanani, A.J., Sherratt, J.A., Norbury, J., Byrne, H.M., 1999. A two parameter family of travelling waves with a singular barrier arising from the modelling of extracellular matrix mediated cellular invasion. *Physica D: Nonlinear Phenomena*. 126, 145–159.
- Saltz, D., Rubenstein, D.I., 1995. Population dynamics of a reintroduced asiatic wild ass (*Equus hemionus*) herd. *Ecological Applications*. 5, 327–335.
- Sewalt, L., Harley, K., van Heijster, P., Balasuriya, S., 2016. Influences of Allee effects in the spreading of malignant tumours. *Journal of Theoretical Biology*. 394, 77–92.
- Simpson, M.J., 2009. Depth-averaging errors in reactive transport modeling. *Water Resources Research*. 45, W02505.
- Simpson, M.J., Landman, K.A., Hughes, B.D., 2009. Multi-species simple exclusion processes. *Physica A: Statistical Mechanics and its Applications*. 388, 399–406.
- Simpson, M.J., Landman, K.A., Hughes, B.D., 2010. Cell invasion with proliferation mechanisms motivated by time-lapse data. *Physica A: Statistical Mechanics and its Applications*. 389, 3779–3790.
- Skellam, J.G., 1951. Random dispersal in theoretical populations. *Biometrika*. 38, 196–218.
- Stephens, P.A., Sutherland, W.J., Freckleton, R.P., 1999. What is the Allee effect? *Oikos*. 87, 185–190.

- Surendran, A., Plank, M.J., Simpson, M.J., 2020. Population dynamics with spatial structure and an Allee effect. *Proceedings of the Royal Society A: Mathematical, Physical and Engineering Sciences.* 476, 20200501.
- Taylor, C.M., Hastings, A., 2005. Allee effects in biological invasions. *Ecology Letters.* 8, 895–908.
- Taylor, N.P., Kim, H., Krause, A.L., Van Gorder, R.A., 2020. A non-local cross-diffusion model of population dynamics I: Emergent spatial and spatiotemporal patterns. *Bulletin of Mathematical Biology.* 82, 112.
- Vortkamp, I., Schreiber, S.J., Hastings, A., Hilker, F.M., 2020. Multiple attractors and long transients in spatially structured populations with an Allee effect. *Bulletin of Mathematical Biology.* 82, 82.
- Zhang, S., Chong, A., Hughes, B.D., 2019. Persistent exclusion processes: Inertia, drift, mixing, and correlation. *Physical Review E.* 100, 042415.